

Performance and Optimization of Network–Coded Cooperative Diversity Systems

Amir Nasri[†], Robert Schober[†], and Murat Uysal^{††}

Department of Electrical and Computer Engineering

[†]University of British Columbia, Canada, ^{††}University of Waterloo, Canada

In this paper, we study network–coded cooperative diversity (NCCD) systems comprising multiple sources, one relay, and one destination where the relay detects the packets received from all sources and performs Galois field network coding. We develop a simple cooperative maximum–ratio combining scheme for the destination which performs close to the optimal maximum–likelihood combining and achieves the maximum diversity gain available in the system. Furthermore, we provide a mathematical framework for performance analysis of NCCD systems for high signal–to–noise ratios in Rayleigh fading. Based on this framework, we derive simple and elegant closed–form expressions for the asymptotic symbol and bit error rates of NCCD systems. The derived error rate expressions are valid for arbitrary number of sources, constellation mappings and modulations, and provide significant insight into the impact of various system and channel parameters on performance. These expressions can also be exploited for mapping optimization as well as for various practically relevant NCCD system optimization problems such as optimal power allocation, relay selection, and relay placement. Simulation results confirm the accuracy of the presented analysis and reveal that the performance of NCCD systems can be considerably improved by optimizing the constellation mapping and the power allocation based on the developed analytical results.

1 Introduction

Cooperative diversity (CD) is an effective technique to exploit the spatial diversity offered by wireless relay nodes. The main drawback of CD schemes is a reduction in throughput as in such systems different cooperating terminals use orthogonal channels for transmission [1]. This throughput reduction is most noticeable in CD systems with multiple source terminals, since the relays forward the signals received by different sources in separate orthogonal channels. As a result each relay can serve only a single source in a given channel slot, and therefore the available channel resources may not be shared among different sources.

One effective approach to increase the throughput in multi-source CD systems is network coding over Galois fields (GFs) [2]–[4]. The idea of network coding was originally developed for wired networks as an efficient routing technique capable of enhancing the network throughput [5]. As this throughput enhancement is achieved by allowing the network relays to simultaneously serve multiple source terminals, the network coding technique is a promising candidate to overcome the throughput bottle-neck in CD systems.

The combination of CD and GF network coding, which is referred to as network-coded CD (NCCD) in this work, has received considerable attention recently. In particular, the outage capacity of such systems was calculated in [2, 3], and their diversity-multiplexing tradeoff was analyzed in [4]. In [6], for a network coding system featuring the algebraic superposition of channel codes and iterative decoding at the destination optimal channel codes were designed based on an ad-hoc code search approach. The diversity order of a NCCD system employing distributed error-correcting codes was analyzed in [7], and it was shown that a maximum diversity order equal to the minimum distance of the employed error-correcting code can be achieved. In addition to GF network coding, physical-layer network coding (PNC) and complex field network coding (CFNC) have been proposed for CD systems in [8] and [9], respectively, which provide additional throughput enhancement but at the cost of high peak-to-average power ratios and stringent time-synchronization requirements.

Common to the works on NCCD systems is the fact that network coding is performed over the GF of order two, thereby limiting the adopted modulation schemes to binary. Furthermore, a general and accurate error rate analysis giving insight into the performance of NCCD systems is not available in the literature. Motivated by this, in this paper, we investigate the error rate performance of a NCCD system with multiple sources employing general M -ary modulation, one relay, and one destination. To develop a simple combining scheme for the destination which yields a performance close to that of the optimal maximum-likelihood (ML) combining and is also amenable to performance

analysis, we generalize the cooperative maximum-ratio combining (C-MRC) scheme in [10] proposed for conventional CD systems. For the resulting NCCD system we derive simple and elegant closed-form expressions for the asymptotic symbol and bit error rates in Rayleigh fading. These closed-form expressions give valuable insight into the impact of various system and channel parameters such as the number of sources and the signal-to-noise ratios (SNRs) of the involved wireless channels. For example, our analytical results reveal that the achieved diversity gain for all source terminals is two irrespective of the number of sources. The network-coding gain, however, depends on the number of source terminals, the employed signal constellation and constellation mapping, and the relevant link qualities. Furthermore, mapping optimization as well as various other NCCD system optimization problems such as optimal power allocation, relay selection, and relay placement can be formulated and solved based on the derived error rate expressions.

The remainder of this paper is organized as follows. In Section 2, the system model for the considered NCCD system as well as some notations and definitions are introduced. Asymptotic expressions for the symbol error rate (SER) and the bit error rate (BER) are derived in Section 3. Optimization of NCCD systems is considered in Section 4 and numerical and simulation results are presented in Section 5. Finally, conclusions are drawn in Section 6.

2 Preliminaries

In this section, we describe the model for the considered NCCD system and introduce some notations and definitions.

2.1 Notations and Definitions

In this paper, $[\cdot]^T$, $(\cdot)^*$, $\Re\{\cdot\}$, $\mathcal{E}_x\{\cdot\}$, and $\Gamma(\cdot)$, denote transposition, complex conjugation, the real part of a complex number, statistical expectation with respect to x , and the Gamma function, respectively. $Q(x) \triangleq \frac{1}{\sqrt{2\pi}} \int_x^\infty e^{-t^2/2} dt$ denotes the Gaussian Q -function. Furthermore, we use the notation $u \stackrel{\circ}{=} v$ to indicate that u and v are asymptotically equivalent, and a function $f(x)$ is $o(g(x))$ if $\lim_{x \rightarrow 0} f(x)/g(x) = 0$.

2.2 Signal Model

The considered NCCD system is depicted in Fig. 1 and comprises N_s source terminals S_i , $1 \leq i \leq N_s$, one relay R , and one destination terminal D . Transmission from the source terminals to the destination terminal is organized in two hops. The first hop comprises N_s orthogonal channel slots, e.g. N_s

different time slots or frequency bands, where each source terminal S_i , $1 \leq i \leq N_s$, transmits its corresponding data to the relay and the destination using one channel slot. In particular, a data symbol $s_i \in \mathcal{A}$ is generated at the source S_i , where $\mathcal{A} \triangleq \text{GF}(2^m)$ is the GF of order $M = 2^m$. This data symbol is mapped to a transmit symbol $x_i \in \mathcal{X}$ with $\mathcal{E}\{|x_i|^2\} = 1$ using the mapping $x_i = \mu_{\mathcal{X}}(s_i)$, where \mathcal{X} denotes an M -ary signal constellation such as M -ary phase-shift keying (M -PSK) or M -ary quadrature amplitude modulation (M -QAM), and $\mu_{\mathcal{X}} : \mathcal{A} \rightarrow \mathcal{X}$ is a one-to-one constellation mapping function from \mathcal{A} to \mathcal{X} . The transmit symbols x_i are then transmitted to the relay and the destination. The signals received by the destination and the relay in the first hop are given by

$$r_{S_i D} = \sqrt{P_i} f_i x_i + n_{D,i}, \quad r_{S_i R} = \sqrt{P_i} g_i x_i + n_{R,i}, \quad (1)$$

for $1 \leq i \leq N_s$, respectively, where P_i is the average transmit power of the i th source, and f_i and g_i denote the fading gains of the $S_i \rightarrow D$ and the $S_i \rightarrow R$ channels, respectively. Furthermore, $n_{D,i}$ and $n_{R,i}$ denote the additive white Gaussian noise (AWGN) samples at the destination and the relay with variances $\sigma_{n_{D,i}}^2 \triangleq \mathcal{E}\{|n_{D,i}|^2\}$ and $\sigma_{n_{R,i}}^2 \triangleq \mathcal{E}\{|n_{R,i}|^2\}$, respectively.

Having received the signals $r_{S_i R}$, the relay performs coherent ML detection to obtain the detected symbols

$$\hat{x}_{R,i} = \arg \min_{\tilde{x} \in \mathcal{X}} \{|r_{S_i R} - \sqrt{P_i} g_i \tilde{x}|^2\}, \quad 1 \leq i \leq N_s. \quad (2)$$

The corresponding detected data symbol is given by $\hat{s}_{R,i} = \mu_{\mathcal{X}}^{-1}(\hat{x}_{R,i}) \in \mathcal{A}$.

The second hop comprises a single channel slot which is orthogonal to those employed in the first hop. In particular, in the second hop the relay performs network coding and computes the data symbol $\hat{s}_R \triangleq \hat{s}_{R,1} \oplus \cdots \oplus \hat{s}_{R,N_s} \in \mathcal{A}$, where \oplus denotes addition in $\text{GF}(2^m)$. The relay then forwards the transmit symbol $\hat{x}_R \triangleq \mu_{\mathcal{X}}(\hat{s}_R) \in \mathcal{X}$ to the destination. The signal received at the destination in the second hop, r_{RD} , can be modeled as

$$r_{RD} = \sqrt{P_R} h_R \hat{x}_R + n_{D,R}, \quad (3)$$

where P_R is the average transmit power of the relay, h_R is the fading gain of the $R \rightarrow D$ channel, and $n_{D,R}$ is the AWGN at the destination in the second hop having variance $\sigma_{n_{D,R}}^2 \triangleq \mathcal{E}\{|n_{D,R}|^2\}$.

Throughout this paper we assume independent Rayleigh fading for all links of the network. Thus, the fading gains $f_i \triangleq a_{f_i} e^{-j\theta_{f_i}}$, $h_i \triangleq a_{g_i} e^{-j\theta_{g_i}}$, $1 \leq i \leq N_s$, and $h_R \triangleq a_{h_R} e^{-j\theta_{h_R}}$, are independent Gaussian random variables (RVs) with zero mean and variances $\Omega_{f_i} \triangleq \mathcal{E}\{|f_i|^2\}$, $\Omega_{g_i} \triangleq \mathcal{E}\{|g_i|^2\}$, $1 \leq i \leq N_s$, and $\Omega_R \triangleq \mathcal{E}\{|h_R|^2\}$, respectively. Here, the channel amplitudes a_{f_i} , a_{g_i} , and a_{h_R} are positive real RVs and follow a Rayleigh distribution. Furthermore, the channel phases θ_{f_i} , θ_{g_i} , and θ_{h_R} are uniformly distributed in $[-\pi, \pi)$ and are independent from the channel amplitudes.

For future reference, we define the instantaneous SNRs of the $S_i \rightarrow D$, $S_i \rightarrow R$, and $R \rightarrow D$ links as $\gamma_{f_i} \triangleq P_i a_{f_i}^2 / \sigma_{n_{D,i}}^2$, $\gamma_{g_i} \triangleq P_i a_{g_i}^2 / \sigma_{n_{R,i}}^2$, and $\gamma_{h_R} \triangleq P_R a_{h_R}^2 / \sigma_{n_R}^2$, respectively. The corresponding average SNRs are given by $\bar{\gamma}_{f_i} = P_i \Omega_{f_i} / \sigma_{n_{D,i}}^2$, $\bar{\gamma}_{g_i} = P_i \Omega_{g_i} / \sigma_{n_{R,i}}^2$, and $\bar{\gamma}_{D,R} = P_R \Omega_R / \sigma_{n_{D,R}}^2$, respectively.

Remark 1: Based on the presented signal model, a total of $N_s + 1$ channel slots are required for the transmission of signals from all sources to the destination. In contrast, a conventional CD system [1, 10] requires $2N_s$ channel slots since the relay assists only a single source in a certain slot.

2.3 Equivalent Source–Relay Channel

In this subsection, we introduce an equivalent channel between the source terminals and the relay for the considered NCCD system which will be particularly useful for developing the diversity combining scheme in Section 2.4 and the performance analysis in Section 3. The input of this equivalent channel, x_R , is the relay transmit symbol in the absence of noise, i.e., $x_R \triangleq \mu_{\mathcal{X}}(s_R) \in \mathcal{X}$ with $s_R \triangleq s_1 \oplus \cdots \oplus s_{N_s} \in \mathcal{A}$, and the output is the actual relay transmit symbol \hat{x}_R . Defining the source–relay SNR vector $\gamma_g \triangleq [\gamma_{g_1}, \dots, \gamma_{g_{N_s}}]^T$, this channel is characterized by the equivalent error probability $P_{e,\text{eq}}(\gamma_g) \triangleq \Pr\{\hat{x}_R \neq x_R\}$. For an M -ary signal constellation \mathcal{X} , the equivalent error probability $P_{e,\text{eq}}(\gamma_g)$ is given by $P_{e,\text{eq}}(\gamma_g) = \beta Q(\sqrt{2\alpha\gamma_{\text{eq}}(\gamma_g)})$, where α and β are two modulation dependent constants (e.g. $\alpha = \beta = 1$ for BPSK). Furthermore, $\gamma_{\text{eq}}(\gamma_g)$ is the instantaneous SNR associated with the equivalent source–relay channel which can be expressed as $\gamma_{\text{eq}}(\gamma_g) = \frac{1}{2\alpha} (Q^{-1}(P_{e,\text{eq}}(\gamma_g)/\beta))^2$. It is not difficult to see that for sufficiently high SNR $\gamma_{\text{eq}}(\gamma_g)$ can be accurately approximated as $\gamma_{\text{eq}}(\gamma_g) = \min\{\gamma_{g_1}, \dots, \gamma_{g_{N_s}}\}$. As a result, since γ_{g_i} , $1 \leq i \leq N_s$, is an exponentially distributed RV with mean $\bar{\gamma}_{g_i}$, $\gamma_{\text{eq}}(\gamma_g)$ is also exponentially distributed with mean $\bar{\gamma}_{\text{eq}} = (1/\bar{\gamma}_{g_1} + \cdots + 1/\bar{\gamma}_{g_{N_s}})^{-1}$.

2.4 Diversity Combining at the Destination

ML combining can be employed at the destination to optimally combine the signals received from the sources and the relay. However, due to the possibility of erroneous decisions at the relay, the ML decision metric is highly complex and not amenable to analysis. In order to avoid the problems associated with the ML metric, we generalize the C–MRC scheme proposed in [10] for conventional CD to NCCD. As will be shown in Section 3, this simple C–MRC scheme performs close to the ML combining and achieves the full diversity of NCCD systems with any number of sources. The

corresponding decision metric for the generalized C-MRC can be written as

$$m_c(\tilde{\mathbf{x}}) = \sum_{i=1}^{N_s} \frac{|r_{S_iD} - \sqrt{P_i} f_i \tilde{x}_i|^2}{\sigma_{n_{D,i}}^2} + \lambda_R \frac{|r_{RD} - \sqrt{P_R} h_R \tilde{x}_R|^2}{\sigma_{n_{D,R}}^2} \quad (4)$$

Here, vector $\tilde{\mathbf{x}} \triangleq [\tilde{x}_1 \dots \tilde{x}_{N_s}]^T \in \mathcal{X}^{N_s}$ contains trial transmit symbols $\tilde{x}_i = \mu_{\mathcal{X}}(\tilde{s}_i) \in \mathcal{X}$, $1 \leq i \leq N_s$, where $\tilde{s}_i \in \mathcal{A}$, $1 \leq i \leq N_s$, are trial data symbols. Furthermore we have defined $\tilde{x}_R \triangleq \mu_{\mathcal{X}}(\tilde{s}_R) \in \mathcal{X}$ with $\tilde{s}_R \triangleq \tilde{s}_1 \oplus \dots \oplus \tilde{s}_{N_s} \in \mathcal{A}$, and the weighting factor $\lambda_R \in [0, 1]$ is defined as $\lambda_R \triangleq \frac{\min\{\gamma_{eq}(\gamma_g), \gamma_R\}}{\gamma_R}$. For the case that all source-relay channels are perfect, $\lambda_R = 1$ is valid and, as expected, (4) reduces to the conventional MRC. However, if at least one of the source-relay channels is not perfect, the metric in (4) assigns a smaller weight $\lambda_R < 1$ to the signal received from the relay to take into account the effect of possible erroneous decisions at the relay. We further note that in order to compute λ_R , the destination has to know the SNR of the weakest source-relay channel. This SNR is available at the relay for coherent detection and can be forwarded to the destination over a low-rate feedback link.

Based on (4) signal detection at the destination can be performed as $\hat{\mathbf{x}}_D = \arg \min_{\tilde{\mathbf{x}} \in \mathcal{X}^{N_s}} \{m_c(\tilde{\mathbf{x}})\}$, where $\hat{\mathbf{x}}_D \triangleq [\hat{x}_{D,1} \dots \hat{x}_{D,N_s}]^T \in \mathcal{X}^{N_s}$ contains the detected symbols at the destination for all sources and the corresponding decoded data symbols are obtained as $\hat{s}_{D,i} \triangleq \mu_{\mathcal{X}}^{-1}(\hat{x}_{D,i}) \in \mathcal{A}$, $1 \leq i \leq N_s$. We note that the data vectors $\tilde{\mathbf{s}}_e \triangleq [\tilde{s}_1, \dots, \tilde{s}_{N_s}, \tilde{s}_R]^T \in \mathcal{X}^{N_s+1}$ form an $(N_s + 1, N_s)$ single-parity-check block code over $\text{GF}(2^m)$. As a result, the signal detection at the destination can be efficiently implemented using various well-known soft-decision decoding algorithms for block codes available in the literature [11], e.g., Viterbi decoding based on the trellis representation of the corresponding single-parity-check block code [12]. A detailed discussion of such algorithms, however, is beyond the scope and limits of the current paper.

3 Performance Analysis

In this section, we analyze the error rate performance of the considered NCCD system for high SNRs, i.e., $\bar{\gamma}_{f_i}, \bar{\gamma}_{g_i} \rightarrow \infty$, $1 \leq i \leq N_s$, and $\bar{\gamma}_R \rightarrow \infty$. In particular, we develop asymptotic closed-form expressions for the (average) pairwise error probability (PEP), SER, and BER. For convenience, we introduce the source-destination SNR vector $\boldsymbol{\gamma}_f \triangleq [\gamma_{f_1}, \dots, \gamma_{f_{N_s}}]^T$, the normalized noise samples $\bar{n}_{D,i} \triangleq n_{D,i}/\sigma_{n_{D,i}}$, $1 \leq i \leq N_s$, and $\bar{n}_{D,R} \triangleq n_{D,R}/\sigma_{n_{D,R}}$, and the noise vector $\mathbf{n} \triangleq [\bar{n}_{D,1}, \dots, \bar{n}_{D,N_s}, \bar{n}_{D,R}]^T$.

For the i th source the SER, P_s^i , can be accurately upper-bounded using a union-bound on the pairwise error probabilities as

$$P_s^i = \frac{1}{M^{N_s}} \sum_{\mathbf{x} \in \mathcal{X}^{N_s}} \sum_{\tilde{\mathbf{x}} \in \mathcal{B}_i(\mathbf{x})} P(\mathbf{x} \rightarrow \tilde{\mathbf{x}}), \quad (5)$$

where $P(\mathbf{x} \rightarrow \tilde{\mathbf{x}})$ denotes the PEP associated with the pair $(\mathbf{x}, \tilde{\mathbf{x}})$ which is the probability that $\mathbf{x} \triangleq [x_1 \cdots x_{N_s}]^T \in \mathcal{X}^{N_s}$ was transmitted by the sources and $\tilde{\mathbf{x}} = [\tilde{x}_1 \cdots \tilde{x}_{N_s}]^T \in \mathcal{X}^{N_s}$, $\tilde{\mathbf{x}} \neq \mathbf{x}$, was detected at the destination, assuming that \mathbf{x} and $\tilde{\mathbf{x}}$ are the only two possible decision outcomes. Furthermore, the set $\mathcal{B}_i(\mathbf{x})$ in (5) is defined as

$$\mathcal{B}_i(\mathbf{x}) \triangleq \{\tilde{\mathbf{x}} | \tilde{x}_j \in \mathcal{X} - \{x_j\}, j = i, \tilde{x}_j \in \mathcal{X}, j \neq i\}. \quad (6)$$

In the following, we first derive an asymptotic expression for the PEP in Subsection 3.1 and then use the obtained result to develop closed-form expressions for the asymptotic SER and BER in Subsection 3.2.

3.1 Asymptotic Pairwise Error Probability

The PEP for the considered NCCD system can be expressed as

$$P(\mathbf{x} \rightarrow \tilde{\mathbf{x}}) = \Pr\{m_c(\mathbf{x}) > m_c(\tilde{\mathbf{x}})\}. \quad (7)$$

It is convenient to first obtain the PEP conditioned on the instantaneous SNRs γ_f , γ_g , γ_R , and the noise vector \mathbf{n} . To drive such an expression we assume that among the transmit signals x_j , $1 \leq j \leq N_s$, at most one is received in error at the relay. Furthermore, we assumed that if the transmit signal x_j is received erroneously, the erroneous $\hat{x}_{R,j}$ at the relay is a nearest neighbor of x_j , i.e., $\hat{x}_{R,j} \in \mathcal{N}(x_j)$, where set $\mathcal{N}(x)$ contains all nearest neighbors of x in \mathcal{X} . These approximations are well justified for $\bar{\gamma}_{g_j} \rightarrow \infty$, $1 \leq j \leq N_s$, and their accuracy will be confirmed by simulations in Section 5. Based on these assumptions the desired conditional PEP can be expressed as

$$P(\mathbf{x} \rightarrow \tilde{\mathbf{x}} | \gamma_f, \gamma_g, \gamma_R, \mathbf{n}) = \Pr\{\hat{x}_R = x_R\} P(\mathbf{x} \rightarrow \tilde{\mathbf{x}} | x_R, \gamma_f, \gamma_{eq}, \gamma_R, \mathbf{n}) \\ + \sum_{j=1}^{N_s} \frac{1}{|\mathcal{D}_j(\mathbf{x})|} \sum_{\hat{x}_R \in \mathcal{D}_j(\mathbf{x})} \beta Q(\sqrt{2\alpha\gamma_{g_j}}) P(\mathbf{x} \rightarrow \tilde{\mathbf{x}} | \hat{x}_R, \gamma_f, \gamma_{eq}, \gamma_R, \mathbf{n}), \quad (8)$$

where

$$\mathcal{D}_j(\mathbf{x}) \triangleq \{\mu_{\mathcal{X}}(\mu_{\mathcal{X}}^{-1}(\tilde{x}_1) \oplus \cdots \oplus \mu_{\mathcal{X}}^{-1}(\tilde{x}_{N_s})) | \bar{x}_\nu \in \mathcal{N}(x_\nu), \nu = j, \bar{x}_\nu = x_\nu, \nu \neq j\}. \quad (9)$$

Here, for a given transmit vector \mathbf{x} the set $\mathcal{D}_j(\mathbf{x})$ collects all possible values for \hat{x}_R assuming that x_j is received in error at the relay while x_i , $i \neq j$, are received correctly. Furthermore, the conditional PEP $P(\mathbf{x} \rightarrow \tilde{\mathbf{x}} | \bar{x}_R, \gamma_f, \gamma_{eq}, \gamma_R, \mathbf{n})$, $\bar{x}_R \in \{x_R, \hat{x}_R\}$, can be written as

$$P(\mathbf{x} \rightarrow \tilde{\mathbf{x}} | \bar{x}_R, \gamma_f, \gamma_{eq}, \gamma_R, \mathbf{n}) = \Pr\{m_c(\mathbf{x}) > m_c(\tilde{\mathbf{x}}) | \bar{x}_R, \gamma_f, \gamma_{eq}, \gamma_R, \mathbf{n}\} \\ = \Pr\left\{\sum_{i=1}^{N_s} \Delta_{f_i}(x_i, \tilde{x}_i) + \lambda_R \Delta_R(x_R, \tilde{x}_R, \bar{x}_R) < 0 \middle| \gamma_f, \gamma_{eq}, \gamma_R, \mathbf{n}\right\}, \quad (10)$$

where

$$\Delta_{f_i}(x_i, \tilde{x}_i) \triangleq |\sqrt{\gamma_{f_i}}(\tilde{x}_i - x_i) + \bar{n}_{D,i}|^2 - |\bar{n}_{D,i}|^2, \quad (11)$$

and

$$\Delta_R(x_R, \tilde{x}_R, \bar{x}_R) \triangleq |\sqrt{\gamma_R}(\tilde{x}_R - \bar{x}_R) + \bar{n}_{D,R}|^2 - |\sqrt{\gamma_R}(x_R - \bar{x}_R) + \bar{n}_{D,R}|^2. \quad (12)$$

For derivation of the unconditional PEP, we exploit that for any RV Δ we have $\Pr\{\Delta < 0\} = \frac{1}{2\pi j} \int_{c-j\infty}^{c+j\infty} \Phi_{\Delta}(s) \frac{ds}{s}$ with moment generating function (MGF) $\Phi_{\Delta}(s) \triangleq \mathcal{E}_{\Delta}\{e^{-\Delta s}\}$ and use the fact that $\Pr\{\hat{x}_R = x_R\} = 1 - P_{e,\text{eq}}(\gamma_g) = 1 - \beta Q(\sqrt{2\alpha\gamma_{\text{eq}}})$, cf. Subsection 2.3. Using these relations, we obtain the unconditional PEP from (8) and (10) as

$$P(\mathbf{x} \rightarrow \tilde{\mathbf{x}}) = \mathcal{E}_{\gamma_f, \gamma_g, \gamma_R, \mathbf{n}} \{P(\mathbf{x} \rightarrow \tilde{\mathbf{x}} | \gamma_f, \gamma_g, \gamma_R, \mathbf{n})\} = \frac{1}{2\pi j} \int_{c-j\infty}^{c+j\infty} \left(\prod_{i=1}^{N_s} \Phi_{f_i}(s) \right) \Phi_R(s) \frac{ds}{s}, \quad (13)$$

where c is a small positive constant that lies in the region of convergence of the integrand and

$$\Phi_{f_i}(s) \triangleq \mathcal{E}_{\gamma_{f_i}, \bar{n}_{D,i}} \{e^{-s\Delta_{f_i}(x_i, \tilde{x}_i)}\}, \quad (14)$$

$$\Phi_R(s) \triangleq \Phi_R^c(s) + \sum_{j=1}^{N_s} \frac{1}{|\mathcal{D}_j(\mathbf{x})|} \sum_{\hat{x}_R \in \mathcal{D}_j(\mathbf{x})} \Phi_{R,j}^e(\hat{x}_R; s). \quad (15)$$

with $\Phi_{R,j}^e(\hat{x}_R; s)$ and $\Phi_R^c(s)$ defined in Lemmas 2 and 4 in the Appendix, respectively. Based on (13) and (15) the PEP can be written as

$$P(\mathbf{x} \rightarrow \tilde{\mathbf{x}}) = P_c(\mathbf{x}, \tilde{\mathbf{x}}) + \sum_{j=1}^{N_s} \frac{1}{|\mathcal{D}_j(\mathbf{x})|} \sum_{\hat{x}_R \in \mathcal{D}_j(\mathbf{x})} P_{e,j}(\mathbf{x}, \tilde{\mathbf{x}}, \hat{x}_R) \quad (16)$$

where

$$P_c(\mathbf{x}, \tilde{\mathbf{x}}) \triangleq \frac{1}{2\pi j} \int_{c-j\infty}^{c+j\infty} \left(\prod_{i=1}^{N_s} \Phi_{f_i}(s) \right) \Phi_R^c(s) \frac{ds}{s}, \quad (17)$$

and

$$P_{e,j}(\mathbf{x}, \tilde{\mathbf{x}}, \hat{x}_R) \triangleq \frac{1}{2\pi j} \int_{c-j\infty}^{c+j\infty} \left(\prod_{i=1}^{N_s} \Phi_{f_i}(s) \right) \Phi_{R,j}^e(\hat{x}_R; s) \frac{ds}{s}. \quad (18)$$

To facilitate the calculation of the asymptotic PEP, we now present the following proposition which sheds some light on the asymptotic characteristics of the PEP $P(\mathbf{x} \rightarrow \tilde{\mathbf{x}})$ (refer to the Appendix for a proof).

Proposition 1: Assume without loss of generality that $\bar{\gamma}_{f_i} = \zeta_{f_i} \bar{\gamma}$, $\bar{\gamma}_{g_i} = \zeta_{g_i} \bar{\gamma}$, $1 \leq i \leq N_s$, and $\bar{\gamma}_R = \zeta_R \bar{\gamma}$, where ζ_{f_i} , ζ_{g_i} and ζ_R are finite (positive) constants, which are independent of $\bar{\gamma}$, and

define the diversity gain associated with the PEP as $G_{d,\text{PEP}} \triangleq -\lim_{\bar{\gamma} \rightarrow \infty} \log(P(\mathbf{x} \rightarrow \tilde{\mathbf{x}})) / \log(\bar{\gamma})$. The diversity gain is then given by $G_{d,\text{PEP}} = d_H(\mathbf{x}, \tilde{\mathbf{x}})$, where $d_H(\mathbf{x}, \tilde{\mathbf{x}})$ denotes the Hamming distance between data vector $\mathbf{s}_e \triangleq [s_1, \dots, s_{N_s}, s_R]^T \in \mathcal{X}^{N_s+1}$ and $\tilde{\mathbf{s}}_e = [\tilde{s}_1, \dots, \tilde{s}_{N_s}, \tilde{s}_R]^T \in \mathcal{X}^{N_s+1}$. Furthermore, for all possible pairs $(\mathbf{x}, \tilde{\mathbf{x}})$ we have $d_H(\mathbf{x}, \tilde{\mathbf{x}}) \geq 2$.

The above proposition reveals that for calculation of the asymptotic SER based on (5), only error events with $d_H(\mathbf{x}, \tilde{\mathbf{x}}) = 2$ should be included since error events with $d_H(\mathbf{x}, \tilde{\mathbf{x}}) > 2$ yield a higher diversity gain and thus, their contribution to the asymptotic SER is negligible. We therefore in the following calculate the asymptotic PEP only for error events with $d_H(\mathbf{x}, \tilde{\mathbf{x}}) = 2$. For clarity, we consider the cases $x_R \neq \tilde{x}_R$ and $x_R = \tilde{x}_R$ separately.

Case 1, $x_R \neq \tilde{x}_R$: It is easy to see that in this case $d_j \triangleq |x_j - \tilde{x}_j|$, $1 \leq j \leq N_s$, is non-zero only for a single value of the index j , i.e., we have $d_j \neq 0$, $j = i$, and $d_j = 0$, $j \neq i$. As a result, from Lemma 1 we obtain $\Phi_{f_j}(s) \triangleq \frac{1}{4s(1-s)\bar{\gamma}_{f_j}}$, $j = i$ and $\Phi_{f_j}(s) \triangleq 1$, $j \neq i$. Therefore, using (17) and Lemma 4 we arrive at

$$P_c(\mathbf{x}, \tilde{\mathbf{x}}) \triangleq \frac{1}{2\pi^2 j} \int_0^{\pi/2} \int_{c-j\infty}^{c+j\infty} \frac{1}{d_i^2 s(1-s)\bar{\gamma}_{f_i}} \left(\frac{2}{\bar{\gamma}_{\text{eq}} d_R^2 s} + \frac{2}{\bar{\gamma}_R d_R^2 s(1-s)} - \frac{\beta}{\bar{\gamma}_{\text{eq}} d_R^2 (s + \frac{\alpha}{\sin^2 \theta d_R^2})} \right) \frac{ds}{s} d\theta. \quad (19)$$

The inner complex integral in (19) can be calculated using the standard inverse Laplace transform techniques such as partial fraction expansion. This yields

$$P_c(\mathbf{x}, \tilde{\mathbf{x}}) \triangleq \frac{1}{\bar{\gamma}_{f_i}} \left(\phi_c^g(\mathbf{x}, \tilde{\mathbf{x}}) \sum_{i=1}^{N_s} \frac{1}{\bar{\gamma}_{g_i}} + \frac{\phi_c^R(\mathbf{x}, \tilde{\mathbf{x}})}{\bar{\gamma}_R} \right), \quad (20)$$

where

$$\phi_c^g(\mathbf{x}, \tilde{\mathbf{x}}) \triangleq \frac{2 - \beta + \frac{\beta \alpha}{\sqrt{\alpha^2 + \alpha d_R^2}}}{2d_i^2 d_R^2}, \quad \phi_c^R(\mathbf{x}, \tilde{\mathbf{x}}) \triangleq \frac{3}{d_i^2 d_R^2}. \quad (21)$$

Furthermore, from (18) and Lemma 2 we have

$$P_{e,j}(\mathbf{x}, \tilde{\mathbf{x}}, \hat{x}_R) \triangleq \frac{\beta}{2\pi^2 j} \int_0^{\pi/2} \int_{c-j\infty}^{c+j\infty} \frac{1}{d_i^2 s^2(1-s)(\bar{d}_R(\hat{x}_R)s + \frac{\alpha}{\sin^2 \theta})\bar{\gamma}_{f_i}\bar{\gamma}_{g_j}} ds d\theta = \frac{\phi_e(\mathbf{x}, \tilde{\mathbf{x}}, \hat{x}_R)}{\bar{\gamma}_{f_i}\bar{\gamma}_{g_j}}, \quad (22)$$

with

$$\phi_e(\mathbf{x}, \tilde{\mathbf{x}}, \hat{x}_R) = \begin{cases} \frac{\beta}{2d_i^2 \bar{d}_R(\hat{x}_R)} - \frac{\beta \alpha}{2d_i^2 \bar{d}_R(\hat{x}_R) \sqrt{\alpha^2 + \alpha \bar{d}_R(\hat{x}_R)}} & \bar{d}_R(\hat{x}_R) > 0 \\ \frac{\beta}{4\alpha d_i^2} - \frac{3\beta \bar{d}_R(\hat{x}_R)}{16d_i^2 \alpha^2} & \bar{d}_R(\hat{x}_R) \leq 0 \end{cases} \quad (23)$$

Case 2, $x_R = \tilde{x}_R$: In this case d_j is non-zero for two values of the index j , i.e., we have $d_j \neq 0$,

$j = i_1, i_2$, and $d_j = 0$, otherwise. Using Lemma 1 then results in $\Phi_{f_j}(s) \triangleq \frac{1}{4s(1-s)\bar{\gamma}_{f_j}}$, $j = i_1, i_2$, and $\Phi_{f_j}(s) \triangleq 1$, otherwise. Furthermore, in this case $d_R = 0$ is valid, and therefore based on Lemma 4 we obtain $\Phi_R^c(s) \triangleq 1$. Thus, using (17) we can write

$$P_c(\mathbf{x}, \tilde{\mathbf{x}}) \triangleq \frac{1}{2\pi^2 j} \int_0^{\pi/2} \int_{c-j\infty}^{c+j\infty} \frac{1}{d_{i_1}^2 d_{i_2}^2 s^3 (1-s)^2 \bar{\gamma}_{f_{i_1}} \bar{\gamma}_{f_{i_2}}} ds d\theta = \frac{\bar{\phi}_c(\mathbf{x}, \tilde{\mathbf{x}})}{\bar{\gamma}_{f_{i_1}} \bar{\gamma}_{f_{i_2}}}, \quad (24)$$

with $\bar{\phi}_c(\mathbf{x}, \tilde{\mathbf{x}}) \triangleq \frac{3}{d_{i_1}^2 d_{i_2}^2}$. Furthermore, from (18) and Lemma 2 we obtain

$$P_{e,j}(\mathbf{x}, \tilde{\mathbf{x}}, \hat{x}_R) \triangleq \frac{1}{2\pi^2 j} \int_0^{\pi/2} \int_{c-j\infty}^{c+j\infty} \frac{\beta}{d_{i_1}^2 d_{i_2}^2 s^3 (1-s)^2 (\bar{d}_R(\hat{x}_R)s + \frac{\alpha}{\sin^2 \theta}) \bar{\gamma}_{f_{i_1}} \bar{\gamma}_{f_{i_2}} \bar{\gamma}_{g_j}} ds d\theta = \frac{\bar{\phi}_e(\mathbf{x}, \tilde{\mathbf{x}}, \hat{x}_R)}{\bar{\gamma}_{f_{i_1}} \bar{\gamma}_{f_{i_2}} \bar{\gamma}_{g_j}}, \quad (25)$$

where $\bar{\phi}_e(\mathbf{x}, \tilde{\mathbf{x}}, \hat{x}_R)$ is a (positive) finite constant which depends on \mathbf{x} , $\tilde{\mathbf{x}}$, and \hat{x}_R .

With these asymptotic expressions for $P_c(\mathbf{x}, \tilde{\mathbf{x}})$ and $P_{e,j}(\mathbf{x}, \tilde{\mathbf{x}}, \hat{x}_R)$ at hand, a closed-form expression for the asymptotic PEP can be calculated based on (16).

3.2 Asymptotic SER and BER

In order to obtain an expression for the asymptotic SER, we first expurgate the union-bound in (5) according to proposition 1. In particular, we only include the error events with $d_H(\mathbf{x}, \tilde{\mathbf{x}}) = 2$ in the union-bound since the contribution of error events with $d_H(\mathbf{x}, \tilde{\mathbf{x}}) > 2$ to the asymptotic SER is negligible (cf. Proposition 1). This expurgation is accomplished by modifying the set $\mathcal{B}_i(\mathbf{x})$ in (6) as

$$\mathcal{C}_i(\mathbf{x}) \triangleq \{\tilde{\mathbf{x}} | \tilde{x}_j \in \mathcal{X} - \{x_j\}, j = i, \tilde{x}_j \in \mathcal{X}, j \neq i, d_H(\mathbf{x}, \tilde{\mathbf{x}}) = 2\}. \quad (26)$$

We are now ready to state our main result. In particular, in the following proposition we use (5) and (26) along with (16) to obtain a general expression for the asymptotic SER which is valid for arbitrary number of sources, arbitrary signal constellations (modulations) and arbitrary constellation mappings (refer to the Appendix for a proof).

Proposition 2: For the NCCD system described in Section 2, the asymptotic SER for the i th source is given by

$$P_s^i \triangleq \frac{1}{\bar{\gamma}_{f_i}} \left(\sum_{i=1}^{N_s} \frac{C_{g_i}}{\bar{\gamma}_{g_i}} + \sum_{\substack{j=1 \\ j \neq i}}^{N_s} \frac{C_{f_j}}{\bar{\gamma}_{f_j}} + \frac{C_R}{\bar{\gamma}_R} \right), \quad (27)$$

where

$$C_{g_i} \triangleq \frac{1}{M^{N_s}} \sum_{\mathbf{x} \in \mathcal{X}^{N_s}} \sum_{\tilde{\mathbf{x}} \in \mathcal{C}_i^i(\mathbf{x})} \left(\phi_c^g(\mathbf{x}, \tilde{\mathbf{x}}) + \frac{1}{|\mathcal{D}_j(\mathbf{x})|} \sum_{\hat{x}_R \in \mathcal{D}_j(\mathbf{x})} \phi_e(\mathbf{x}, \tilde{\mathbf{x}}, \hat{x}_R) \right), \quad (28)$$

$$C_{f_j} \triangleq \frac{1}{M^{N_s}} \sum_{\mathbf{x} \in \mathcal{X}^{N_s}} \sum_{\tilde{\mathbf{x}} \in \mathcal{C}_i^j(\mathbf{x})} \bar{\phi}_c(\mathbf{x}, \tilde{\mathbf{x}}). \quad (29)$$

and

$$C_R \triangleq \frac{1}{M^{N_s}} \sum_{\mathbf{x} \in \mathcal{X}^{N_s}} \sum_{\tilde{\mathbf{x}} \in \mathcal{C}_i^i(\mathbf{x})} \phi_c^R(\mathbf{x}, \tilde{\mathbf{x}}), \quad (30)$$

In (28)–(29), $\mathcal{C}_i^l(\mathbf{x})$, $1 \leq l \leq N_s$, is defined as

$$\mathcal{C}_i^l(\mathbf{x}) \triangleq \{\tilde{\mathbf{x}} | \tilde{x}_j \neq x_j, j = i, l, \tilde{x}_j = x_j, \text{ otherwise, } d_H(\mathbf{x}, \tilde{\mathbf{x}}) = 2\}. \quad (31)$$

Remark 2: The asymptotic SER in (27) is, in general, a function of the constellation mapping $\mu_{\mathcal{X}}$ as the sets $\mathcal{C}_i^l(\mathbf{x})$ and $\mathcal{D}_j(\mathbf{x})$ and consequently the coefficients C_{g_j} , C_{f_j} , and C_R depend on the type of mapping. We shall study this dependency in Section 5 and show that some performance improvement is possible by optimizing the mapping $\mu_{\mathcal{X}}$. In the case of BPSK constellation, however, it can be shown that the only two possible mappings are equivalent and lead to the same expression for the asymptotic SER. Specifically, for BPSK constellation the asymptotic BER (which is equivalently given by the asymptotic SER) can be obtained based on (27) as

$$P_{b,\text{BPSK}}^i \triangleq \frac{1}{\bar{\gamma}_{f_i}} \left(C_{\text{BPSK}}^1 \sum_{i=1}^{N_s} \frac{1}{\bar{\gamma}_{g_i}} + C_{\text{BPSK}}^2 \left[\sum_{\substack{j=1 \\ j \neq i}}^{N_s} \frac{1}{\bar{\gamma}_{f_j}} + \frac{1}{\bar{\gamma}_R} \right] \right), \quad (32)$$

independent of the mapping $\mu_{\mathcal{X}}$, where $C_{\text{BPSK}}^1 \triangleq \frac{45+\sqrt{5}}{160}$ and $C_{\text{BPSK}}^2 \triangleq \frac{3}{16}$.

Remark 3: Letting $\bar{\gamma}_{f_i} = \zeta_{f_i} \bar{\gamma}$, $\bar{\gamma}_{g_i} = \zeta_{g_i} \bar{\gamma}$, $1 \leq i \leq N_s$, and $\bar{\gamma}_R = \zeta_R \bar{\gamma}$, where ζ_{f_i} , ζ_{g_i} and ζ_R are finite (positive) constants, we can express the asymptotic SER of the i th source as $P_{s,\mathcal{X}}^i \triangleq (G_{c,\text{SER}}^i \bar{\gamma})^{-G_{d,\text{SER}}^i}$, where $G_{d,\text{SER}}^i$ and $G_{c,\text{SER}}^i$ are the *diversity gain* and the *network-coding gain* corresponding to the asymptotic SER, respectively. Thus, $G_{d,\text{SER}}^i$ and $G_{c,\text{SER}}^i$ correspond to the negative asymptotic slope and a relative horizontal shift of the SER curve when plotted as a function of $\bar{\gamma}$ on a double-logarithmic scale, respectively. Based on (27) we therefore obtain

$$G_{d,\text{SER}}^i = 2, \quad G_{c,\text{SER}}^i[\text{dB}] = 5 \log_{10}(\zeta_{f_i}) - 5 \log_{10} \left(\sum_{i=1}^{N_s} \frac{C_{g_i}}{\zeta_{g_i}} + \sum_{\substack{j=1 \\ j \neq i}}^{N_s} \frac{C_{f_j}}{\zeta_{f_j}} + \frac{C_R}{\zeta_R} \right). \quad (33)$$

From (33) it is evident that $G_{d,\text{SER}}^i = 2$ is achieved irrespective of the number of sources N_s . Furthermore, for the network-coding gain, $G_{c,\text{SER}}^i$, the following observations are in order. $G_{c,\text{SER}}^i$ is a function of the number of sources N_s , the signal constellation \mathcal{X} , the constellation mapping $\mu_{\mathcal{X}}$, as well as the relative link qualities ζ_{f_i} , ζ_{g_i} , and ζ_R . Letting $\zeta_{f_i} = \zeta_{g_i} = \zeta_R$ in (33) reveals that the network-coding gain only logarithmically increases with increasing N_s . Furthermore, it is observed that

for a NCCD system where the relay–destination link is a bottle-neck, i.e., $\zeta_R \ll \zeta_{f_i}, \zeta_{g_i}, 1 \leq i \leq N_s$, $G_{c,\text{SER}}^i$ can be approximate as $G_{c,\text{SER}}^i \approx 5 \log_{10}(\zeta_{f_i} \zeta_R / C_R)$, implying that the network-coding gain is approximately independent of the number of sources. The above observations will be confirmed in Section 5 via simulation results.

Remark 4: Having obtained the asymptotic SER from (27), for Gray labeling, the asymptotic BER of the i th source, P_b^i , can be tightly approximated as $P_b^i \triangleq \frac{1}{\log_2(M)} P_s^i$.

4 Optimization of NCCD Systems

In addition to the mapping optimization discussed in the previous section, the obtained analytical performance results can be employed to formulate various practically relevant optimization problems for NCCD systems. In this section, due to space limitations we only consider the problem of optimal power allocation (OPA), but bare in mind that other optimization problems such as optimal relay selection and optimal relay placement can be treated in a similar manner [13]. In particular, in this section we investigate the optimal allocation of the source and relay powers, P_i , $1 \leq i \leq N_s$, and P_R in a NCCD system for a given total power budget. In Section 5, we will show that such optimal power allocation can lead to significant improvement in the performance of NCCD systems.

Based on the asymptotic SER given in (27), the OPA optimization problem can be mathematically cast as

$$\min_{P_1, \dots, P_{N_s}, P_R} \sum_{i=1}^{N_s} \psi_i \left(\frac{1}{P_i \xi_{f_i}} \left[\sum_{i=1}^{N_s} \frac{C_{g_i}}{P_i \xi_{g_i}} + \sum_{\substack{j=1 \\ j \neq i}}^{N_s} \frac{C_{f_j}}{P_j \xi_{f_j}} + \frac{C_R}{P_R \xi_R} \right] \right) \quad (34a)$$

$$\text{subject to : } \sum_{i=1}^{N_s} P_i + P_R \leq P_t \quad (34b)$$

$$0 \leq P_i \leq P_{i,\max}, \quad 1 \leq i \leq N_s \quad (34c)$$

$$0 \leq P_R \leq P_{R,\max}, \quad (34d)$$

where $\psi_i(\cdot)$ is an increasing convex cost function, P_t is the total power budget, $P_{i,\max}$ and $P_{R,\max}$ denote the maximum power available at the i th source and the relay, respectively, and we have defined the link statistics $\xi_{f_i} \triangleq \Omega_{f_i} / \sigma_{n_{D,i}}^2$, $\xi_{g_i} \triangleq \Omega_{g_i} / \sigma_{n_{R,i}}^2$, and $\xi_R \triangleq \Omega_R / \sigma_{n_R}^2$, respectively.

It is easy to see that the solution set of the linear constraints (34b)–(34d) is non-empty, and therefore the optimization problem is always feasible. In addition, using the transformation of variables $P_i = \log(\tilde{P}_i)$, $1 \leq i \leq N_s$, $P_R = \log(\tilde{P}_R)$, the optimization problem of (34) can be transform into a convex optimization problem in the new variables \tilde{P}_i and \tilde{P}_R which can be subsequently solved globally

using convex optimization methods. We furthermore note that as customary in the literature, here we assume that the power allocation is implemented at the destination node and this node notifies the sources and the relay node of their assigned transmission power. To solve the optimization problem in (34), the destination requires the knowledge about the channel statistics ξ_{f_i} , ξ_{g_i} , $1 \leq i \leq N_s$, and ξ_R . The destination can easily estimate ξ_{f_i} , $1 \leq i \leq N_s$, and ξ_R , as the required information is already available at the destination. ξ_{g_i} , $1 \leq i \leq N_s$, can be similarly estimated by relay and then fed back to the destination via a low-rate feedback link.

For the cost function $\psi_i(\cdot)$, of particular interest are two special cases, $\psi_i(x) = x$ and $\psi_i(x) = \exp(\rho x)$, $\rho \rightarrow \infty$, which lead to average-SER based OPA and min-max fair OPA, respectively. For the scenario considered in this paper, the latter is practically more appealing as it is well known that average-SER based OPA can be biased towards sources with best link qualities and therefore may be unfair to the other sources [14]. Therefore, in the following we consider the min-max fair OPA which aims at minimizing the maximum SER among all sources. In particular, letting $\psi_i(x) = \exp(\rho x)$, $\rho \rightarrow \infty$, in (34) this power allocation optimization problem can be formulated as

$$\min_{P_1, \dots, P_{N_s}, P_R} \max_i \left\{ \frac{1}{P_i \xi_{f_i}} \left[\sum_{i=1}^{N_s} \frac{C_{g_i}}{P_i \xi_{g_i}} + \sum_{\substack{j=1 \\ j \neq i}}^{N_s} \frac{C_{f_j}}{P_j \xi_{f_j}} + \frac{C_R}{P_R \xi_R} \right] \right\} \quad (35a)$$

$$\text{subject to :} \quad \text{The constraints (34b) – (34d)}. \quad (35b)$$

Introducing an auxiliary variable ν , this optimization problem can be equivalently expressed as

$$\min_{P_1, \dots, P_{N_s}, P_R, \nu \geq 0} \nu \quad (36a)$$

$$\text{subject to :} \quad \frac{1}{P_i \xi_{f_i}} \left[\sum_{i=1}^{N_s} \frac{C_{g_i}}{P_i \xi_{g_i}} + \sum_{\substack{j=1 \\ j \neq i}}^{N_s} \frac{C_{f_j}}{P_j \xi_{f_j}} + \frac{C_R}{P_R \xi_R} \right] \leq \nu, \quad 1 \leq i \leq N_s \quad (36b)$$

$$\text{The constraints (34b) – (34d)}. \quad (36c)$$

Since in (36) the objective and constraint functions can be written in the form of posynomials, the optimization problem in (36) is a geometric program (GP) which can be efficiently solved using GP tools [15, 14].

5 Results and System Optimization

In this section, we verify the analytical results derived in Section 3 with computer simulations and employ these results to study and optimize the performance of NCCD systems. In all figures for BPSK

modulation the asymptotic BER is obtained based on (32), while for constellations with higher order the asymptotic SER is obtained using (27).

5.1 Performance of NCCD Systems

In Fig. 2, we consider the BER performance of a NCCD system with $N_s = 2$ sources and BPSK modulation for various settings of the involved channel qualities. For this system $\bar{\gamma}_{f_1} = \bar{\gamma}_{f_2} \triangleq \bar{\gamma}_f$ and $\bar{\gamma}_{g_1} = \bar{\gamma}_{g_2} \triangleq \bar{\gamma}_g$ are assumed, and the results are shown for four combinations of channel qualities $(\bar{\gamma}_f, \bar{\gamma}_g, \bar{\gamma}_R)$. Due to the symmetry of the network, the BER results obtained for the two sources are equal and therefore only the average BER of the two sources are shown. As observed from the figure, the analytical results are in excellent agreement with the simulation results for sufficiently high SNR, confirming the accuracy of the approximations made in Section 2 and 3. As expected from the analysis in Section 3 (cf. Remark 3), the network-coding gain is a function of the respective channels qualities, but nevertheless, a diversity gain of two is achieved for all channel quality combinations. Also shown in this figure are the simulated BER results for ML combining at the destination, which confirm that the performance achieved by the generalized C-MRC scheme is very close to that of the ML combining in all cases.

The BER performance results for an asymmetric NCCD system with $N_s = 4$ sources and BPSK modulation are shown in Fig. 3. For this system we have assumed $\bar{\gamma}_{f_1} \triangleq \bar{\gamma}$, $\bar{\gamma}_{f_2} = \bar{\gamma} + 10$ dB, $\bar{\gamma}_{f_3} = \bar{\gamma} + 16$ dB, $\bar{\gamma}_{f_4} = \bar{\gamma} + 20$ dB and $\bar{\gamma}_{g_1} = \bar{\gamma}_{g_2} = \bar{\gamma}_{g_3} = \bar{\gamma}_{g_4} = \bar{\gamma}_R = \bar{\gamma}$. The BER results for the individual sources as well as the average BER (of all sources) are shown as a function of $\bar{\gamma}$ in this figure. We observe that although all individual sources achieve a diverse order of two, different network-coding gains are achieved by different sources as the network-coding gain depends on the respective channel qualities.

In the next figure we study the impact of number of sources on the performance of NCCD systems. In particular, we consider a NCCD system with $\bar{\gamma}_{f_i} = \bar{\gamma}_{g_i} = \bar{\gamma}$, $1 \leq i \leq N_s$, $\bar{\gamma}_R = \bar{\gamma}$ and show the average BER for different N_s as a function of $\bar{\gamma}$ for BPSK. The analytical results are shown for three values of $\bar{\gamma}_R$, but the simulation results are shown only for two $\bar{\gamma}_R$ values to avoid crowding the figure. As expected, a diversity gain of two is achieved in all cases irrespective of the number of sources. Furthermore, in accordance with our findings in Remark 3 we observe that the network-coding gain only logarithmically increases with N_s . In addition, as $\bar{\gamma}_R$ decreases the network-coding gain becomes less dependent on N_s and is rendered independent of N_s for low enough $\bar{\gamma}_R$. We also note that although increasing N_s results in some performance degradation, increasing this quantity also leads to an increase in the throughput savings (cf. Remark 1) which, in general, more than compensates

for this slight performance loss.

5.2 Performance Optimization

As discussed in Remark 3, the performance of a NCCD system can be optimized by optimizing the constellation mapping $\mu_{\mathcal{X}}$. In Figs. 5 and 6 we consider this mapping optimization problem for a NCCD system with 16-QAM and $N_s = 2$ for two channel quality settings Case I ($\bar{\gamma}_{f_1} = \bar{\gamma}_{f_2} = \bar{\gamma}_R = \bar{\gamma}$, $\bar{\gamma}_{g_1} = \bar{\gamma}_{g_2} = \bar{\gamma} + 30$ dB) and Case II ($\bar{\gamma}_{f_1} = \bar{\gamma}_{f_2} = \bar{\gamma}_{g_1} = \bar{\gamma}_{g_2} = \bar{\gamma}$, $\bar{\gamma}_R = \bar{\gamma} - 30$ dB). For both cases a random search was performed to find the mapping that minimizes the asymptotic SER in (27). The resulting optimal mappings along with a natural mapping are depicted in Fig. 5. The simulated SER as well as the analytical SER results for the optimal and natural mappings are shown in Fig. 6 as a function of $\bar{\gamma}$ for Cases I and II. As seen, for non-binary constellations the agreement between the simulation and analytical results is not as close as in the binary case which is due to the fact that a union-bound is used in (5) to upper-bound the SER. Nevertheless, for both cases the SER upper-bound is able to accurately predict the difference between the simulated SER results for the optimal and natural mappings, suggesting that this upper-bound is a suitable criterion for mapping optimization. In addition, as observed from the figure, in both cases a performance gain of 1 dB is achieved by the optimal mapping compared to the natural mapping. For 8-PSK, a natural mapping as well as optimal mappings for Cases I and II (obtained using a similar approach as above) are shown shown in Fig. 7. Simulation results (not shown) reveal that for both Cases I and II the optimal mappings outperform the natural mapping by 0.8 dB.

In Fig. 8 we consider the min-max fair OPA problem described in Section 4 (cf. Eq. 35) for a NCCD system with BPSK, $N_s = 2$, $\Omega_{f_1} = \Omega_{g_1} = 1$, $\Omega_{f_2} = \Omega_{g_2} = 50$, $\Omega_R = 200$, and $\sigma_{n_{D,i}}^2 = \sigma_{n_{R,i}}^2 = \sigma_{n_{D,R}}^2 \triangleq \sigma^2$. To allow an unobstructed view of the effect of system parameters on the power allocation, we omit the constraints (35b) by letting $P_{i,\max} = \infty$, $i = 1, 2$, and $P_{R,\max} = \infty$. The BERs of both sources S_i , $i \in \{1, 2\}$ as well as the average BER of both sources are shown as a function of P_t/σ^2 , and are compared with that of equal power allocation (EPA), where $P_1 = P_2 = P_R = P_t/3$. Since S_1 has a weaker channel and therefore a higher BER compared to S_2 , the OPA aims at minimizing the BER of S_1 and improves the corresponding BER by 3.5 dB. This performance improvement is achieved by allocating more power to S_1 than to S_2 (and the relay), and is accomplished at the expense of a small degradation in the BER of source S_2 . Fig. 8 further reveals although the average BER was not adopted as the cost function for the optimization problem, this performance measure is also improved by 3.2 dB compared to EPA.

6 Conclusions

In this paper, we studied NCCD systems where the network coding is performed over $\text{GF}(2^m)$ and developed a simple C-MRC diversity combining scheme which achieves the maximum diversity of the considered system even if erroneous decisions at the relay are taken into account. Assuming independent Rayleigh fading for all links in the network, we derived closed-form expressions for the asymptotic SER and BER of the considered NCCD system. These simple and elegant expressions provide insight into the impact of various system and channel parameters on performance and can be exploited for system design and performance optimization. Simulation results confirmed the accuracy of the presented asymptotic SER and BER results and revealed that both mapping optimization and optimal power allocation can considerably improve the performance of NCCD systems.

Appendix

In this appendix, we provide Lemmas 1–4 and prove Propositions 1 and 2.

Lemma 1: The asymptotic behavior of $\Phi_{f_i}(s)$, $1 \leq i \leq N_s$, for $\bar{\gamma}_{f_i} \rightarrow \infty$ is given by

$$\Phi_{f_i}(s) \doteq \frac{1}{d_i^2 s (1-s) \bar{\gamma}_{f_i}}, \quad (37)$$

for $d_i \triangleq |x_i - \tilde{x}_i| \neq 0$ and $\Phi_{f_i}(s) \doteq 1$ for $d_i = 0$.

Proof. This result can be proved following the same steps as in [16, Section IV.A]. Due to space considerations a detailed proof is not provided here. ■

Lemma 2: The asymptotic behavior of $\Phi_{R,j}^e(\hat{x}_R; s) \triangleq \mathcal{E}_{\gamma_g, \gamma_R, \bar{n}_{D,R}} \{ \beta Q [\sqrt{2\alpha} \gamma_{g_j}] e^{-s\lambda_R \Delta_R(x_R, \tilde{x}_R, \hat{x}_R)} \}$ for $\bar{\gamma}_{g_i} \rightarrow \infty$, $1 \leq i \leq N_s$, $\bar{\gamma}_R \rightarrow \infty$ is given by

$$\Phi_{R,j}^e(\hat{x}_R; s) \doteq \frac{1}{\pi} \int_0^{\pi/2} \frac{\beta}{\bar{\gamma}_{g_j} (\bar{d}_R(\hat{x}_R) s + \frac{\alpha}{\sin^2 \theta})} d\theta, \quad (38)$$

where $\bar{d}_R(\hat{x}_R) \triangleq |\tilde{x}_R - \hat{x}_R|^2 - |x_R - \hat{x}_R|^2$.

Proof. Using the alternative representation for the Q-function $Q[x] = \frac{1}{\pi} \int_0^{\pi/2} e^{-x^2/\sin^2 \theta} d\theta$ we can write

$$\Phi_{R,j}^e(\hat{x}_R; s) = \frac{\beta}{\pi} \int_0^{\pi/2} \mathcal{E}_{\bar{n}_{D,R}} \{ \Phi(s, \theta) \} d\theta, \quad (39)$$

where $\Phi(s, \theta) \triangleq \mathcal{E}_{\gamma_g, \gamma_R} \{ e^{-\frac{\alpha \gamma_{g_j}}{\sin^2 \theta}} e^{-s\lambda_R \Delta_R(x_R, \tilde{x}_R, \hat{x}_R)} \}$. Furthermore, from (12) we have

$$\lambda_R \Delta_R(x_R, \tilde{x}_R, \hat{x}_R) = \gamma_m \bar{d}_R(\hat{x}_R) + \frac{2\gamma_m}{\sqrt{\gamma_R}} d_R \Re\{\bar{n}_{D,R}^*\}, \quad (40)$$

with $\gamma_m \triangleq \min\{\gamma_{eq}, \gamma_R\}$. Using the Taylor series expansion $e^x = \sum_{i=0}^{\infty} x^i/i!$ leads to

$$\Phi(s, \theta) = \sum_{i=0}^{\infty} \frac{2^i \eta_i}{(2i)!} |\bar{n}_{D,R}|^{2i} s^{2i} \Psi_i(s, \theta), \quad (41)$$

with $\eta_i \triangleq \frac{\Gamma(i+1/2)}{\sqrt{\pi}\Gamma(i+1)}$ and

$$\begin{aligned}\Psi_i(s, \theta) &\triangleq \mathcal{E}_{\gamma_g, \gamma_R} \left\{ e^{-(\gamma_m \bar{d}_R(\hat{x}_R)s + \frac{\alpha \gamma_{g_j}}{\sin^2 \theta})} \left(\frac{\gamma_m d_R}{\sqrt{\gamma_R}} \right)^{2i} \right\} \\ &= \frac{d_R^{2i}}{\bar{\gamma}_{g_j} \bar{\gamma}_R \bar{\gamma}_u} \int_0^\infty \int_0^\infty \int_0^\infty e^{-(\gamma_m \bar{d}_R(\hat{x}_R)s + \frac{\alpha \gamma_{g_j}}{\sin^2 \theta})} \gamma_m^{2i} \gamma_R^{-i} e^{-\gamma_{g_j}/\bar{\gamma}_{g_j}} e^{-\gamma_R/\bar{\gamma}_R} e^{-\gamma_u/\bar{\gamma}_u} d\gamma_{g_j} d\gamma_R d\gamma_u. \quad (42)\end{aligned}$$

The auxiliary RV γ_u in (42) is defined as $\gamma_u \triangleq \min_{\substack{1 \leq i \leq N_s \\ i \neq j}} \{\gamma_{g_j}\}$, and is thus an exponentially distributed RV with mean $\bar{\gamma}_u = (\sum_{\substack{j=1 \\ j \neq i}}^{N_s} \bar{\gamma}_{g_j}^{-1})^{-1}$. Based on the definition of γ_m we therefore conclude that $\gamma_m = \min\{\gamma_{g_j}, \gamma_u, \gamma_R\}$. It can be shown that among the three possible cases $\gamma_m = \gamma_R$, $\gamma_m = \gamma_u$, and $\gamma_m = \gamma_{g_j}$, the latter dominates the asymptotic behavior of $\Psi_i(s)$ (the proof is omitted due to space limitations). Consequently, we can write $\Psi_i(s) \doteq \Psi_i^1(s) + \Psi_i^2(s)$, where $\Psi_i^1(s)$ and $\Psi_i^2(s)$ correspond to the two cases $\gamma_{g_j} \leq \gamma_R \leq \gamma_u$ and $\gamma_{g_j} \leq \gamma_u \leq \gamma_R$, respectively, and are defined as

$$\Psi_i^1(s, \theta) \triangleq \frac{d_R^{2i}}{\bar{\gamma}_{g_j} \bar{\gamma}_R \bar{\gamma}_u} \int_0^\infty d\gamma_{g_j} e^{-\gamma_{g_j}(\bar{d}_R(\hat{x}_R)s + \frac{\alpha}{\sin^2 \theta} + \frac{1}{\bar{\gamma}_{g_j}})} \gamma_{g_j}^{2i} \int_{\gamma_{g_j}}^\infty d\gamma_u e^{-\gamma_u/\bar{\gamma}_u} \int_{\gamma_{g_j}}^{\gamma_u} d\gamma_R e^{-\gamma_R/\bar{\gamma}_R} \gamma_R^{-i}, \quad (43)$$

and

$$\Psi_i^2(s, \theta) \triangleq \frac{d_R^{2i}}{\bar{\gamma}_{g_j} \bar{\gamma}_R \bar{\gamma}_u} \int_0^\infty d\gamma_{g_j} e^{-\gamma_{g_j}(\bar{d}_R(\hat{x}_R)s + \frac{\alpha}{\sin^2 \theta} + \frac{1}{\bar{\gamma}_{g_j}})} \gamma_{g_j}^{2i} \int_{\gamma_{g_j}}^\infty d\gamma_u e^{-\gamma_u/\bar{\gamma}_u} \int_{\gamma_u}^\infty d\gamma_R e^{-\gamma_R/\bar{\gamma}_R} \gamma_R^{-i}. \quad (44)$$

In the following, we find the asymptotic behavior of $\Psi_i^1(s, \theta)$ and $\Psi_i^2(s, \theta)$ for $\bar{\gamma}_{g_j}, \bar{\gamma}_u, \bar{\gamma}_R \rightarrow \infty$, respectively. For $\Psi_i^1(s, \theta)$, according to (43) we can write

$$\begin{aligned}\Psi_i^1(s, \theta) &= \frac{d_R^{2i}}{\bar{\gamma}_{g_j} \bar{\gamma}_R \bar{\gamma}_u} \int_0^\infty d\gamma_{g_j} e^{-\gamma_{g_j}(\bar{d}_R(\hat{x}_R)s + \frac{\alpha}{\sin^2 \theta} + 1/\bar{\gamma}_{g_j})} \gamma_{g_j}^{2i} \\ &\quad \times \int_{\gamma_{g_j}}^\infty d\gamma_u e^{-\gamma_u/\bar{\gamma}_u} \left[\bar{\gamma}_R^{1-i} \Gamma(1-i, \gamma_{g_j}/\bar{\gamma}_R) - \bar{\gamma}_R^{1-i} \Gamma(1-i, \gamma_u/\bar{\gamma}_R) \right]. \quad (45)\end{aligned}$$

To obtain the asymptotic behavior of $\Psi_i^1(s, \theta)$ we consider three cases $i > 1$, $i = 1$, and $i = 0$, respectively, and employ the asymptotic properties of the incomplete gamma function $\Gamma(\cdot, z)$ for $z \rightarrow 0$ given by

$$\Gamma(-\kappa, z) \doteq \begin{cases} \frac{(-1)^\kappa}{\kappa!} (\psi(\kappa+1) - \log z) + \frac{z^{-\kappa}}{\kappa} & \kappa \geq 1 \\ -\log z - \gamma & \kappa = 0 \end{cases} \quad (46)$$

In particular, for $i > 1$ from (46) we have $\Gamma(1-i, \gamma_{g_j}/\bar{\gamma}_R) = 1/(i-1)(\gamma_{g_j}/\bar{\gamma}_R)^{1-i}$. Therefore (45) reduces to

$$\begin{aligned}\Psi_i^1(s, \theta) &\doteq \frac{d_R^{2i}}{\bar{\gamma}_{g_j} \bar{\gamma}_R \bar{\gamma}_u (i-1)} \int_0^\infty d\gamma_{g_j} e^{-\gamma_{g_j}(\bar{d}_R(\hat{x}_R)s + \frac{\alpha}{\sin^2 \theta} + 1/\bar{\gamma}_{g_j})} \gamma_{g_j}^{2i} \left(\gamma_{g_j}^{1-i} \bar{\gamma}_u - \bar{\gamma}_u^{2-i} \Gamma(2-i, \gamma_{g_j}/\bar{\gamma}_u) \right) \\ &\doteq O(\bar{\gamma}_{g_j}^{-1} \bar{\gamma}_R^{-1}), \quad (47)\end{aligned}$$

where we have again used (46) to obtain the last asymptotic equality.

For $i = 1$ we have $\Gamma(0, \gamma_{g_j}/\bar{\gamma}_R) = -\log(\gamma_{g_j}/\bar{\gamma}_R)$ and therefore (45) can be written as

$$\begin{aligned}\Psi_i^1(s, \theta) &= \frac{d_R^{2i}}{\bar{\gamma}_{g_j} \bar{\gamma}_R \bar{\gamma}_u} \int_0^\infty d\gamma_{g_j} e^{-\gamma_{g_j}(\bar{d}_R(\hat{x}_R)s + \frac{\alpha}{\sin^2 \theta} + 1/\bar{\gamma}_{g_j})} \gamma_{g_j}^2 \left[\int_{\gamma_{g_j}}^\infty d\gamma_u \log \gamma_u e^{-\gamma_u/\bar{\gamma}_u} - \log(\gamma_{g_j}) \bar{\gamma}_u \right] \\ &\doteq O(\bar{\gamma}_{g_j}^{-1} \bar{\gamma}_R^{-1} \log(\bar{\gamma}_u)).\end{aligned}\quad (48)$$

Finally, for $i = 0$, $\Gamma(1, \gamma_{eq}/\bar{\gamma}_R) = 1$ is valid and therefore after using appropriate transformation of variables in (43) we arrive at

$$\begin{aligned}\Psi_i^1(s, \theta) &= \frac{1}{\bar{\gamma}_{g_j} \bar{\gamma}_R \bar{\gamma}_u} \int_0^\infty d\gamma_u \int_0^{\gamma_u} d\gamma_R \int_0^{\gamma_R} d\gamma_{g_j} e^{-(\gamma_{g_j} \bar{d}_R(\hat{x}_R)s + \frac{\alpha \gamma_{g_j}}{\sin^2 \theta})} e^{-\gamma_{g_j}/\bar{\gamma}_{g_j}} e^{-\gamma_R/\bar{\gamma}_R} e^{-\gamma_u/\bar{\gamma}_u}, \\ &= \frac{\bar{\gamma}_u}{\bar{\gamma}_{g_j} (\bar{\gamma}_R + \bar{\gamma}_u) (\bar{d}_R(\hat{x}_R)s + \frac{\alpha}{\sin^2 \theta})}.\end{aligned}\quad (49)$$

For $\Psi_i^2(s, \theta)$ we first write (44) as

$$\Psi_i^2(s, \theta) = \frac{d_R^{2i}}{\bar{\gamma}_{g_j} \bar{\gamma}_R \bar{\gamma}_u} \int_0^\infty d\gamma_{g_j} e^{-\gamma_{g_j}(\bar{d}_R(\hat{x}_R)s + \frac{\alpha}{\sin^2 \theta} + 1/\bar{\gamma}_{g_j})} \gamma_{g_j}^{2i} \int_{\gamma_{g_j}}^\infty d\gamma_u e^{-\gamma_u/\bar{\gamma}_u} \bar{\gamma}_R^{1-i} \Gamma(1-i, \gamma_u/\bar{\gamma}_R). \quad (50)$$

Using an approach similar to that used in obtaining the asymptotic $\Psi_i^1(s, \theta)$, for $i > 1$ we have

$$\Psi_i^2(s, \theta) \doteq \frac{d_R^{2i}}{\bar{\gamma}_{g_j} \bar{\gamma}_R \bar{\gamma}_u (i-1)} \int_0^\infty d\gamma_{g_j} e^{-\gamma_{g_j}(\bar{d}_R(\hat{x}_R)s + \frac{\alpha}{\sin^2 \theta} + 1/\bar{\gamma}_{g_j})} \gamma_{g_j}^{2i} (\bar{\gamma}_u^{2-i} \Gamma(2-i, \gamma_{g_j}/\bar{\gamma}_u)), \quad (51)$$

which leads to $\Psi_i^2(s, \theta) \doteq O(\bar{\gamma}_{g_j}^{-1} \bar{\gamma}_R^{-1} \bar{\gamma}_u^{-1})$ for $i > 2$, and $\Psi_i^2(s, \theta) \doteq O(\bar{\gamma}_{g_j}^{-1} \bar{\gamma}_R^{-1} \bar{\gamma}_u^{-1} \log(\bar{\gamma}_u))$ for $i = 2$.

Furthermore, for $i = 1$ and $i = 0$ we obtain

$$\begin{aligned}\Psi_i^2(s, \theta) &= \frac{d_R^{2i}}{\bar{\gamma}_{g_j} \bar{\gamma}_R \bar{\gamma}_u} \int_0^\infty d\gamma_{g_j} e^{-\gamma_{g_j}(\bar{d}_R(\hat{x}_R)s + \frac{\alpha}{\sin^2 \theta} + 1/\bar{\gamma}_{g_j})} \gamma_{g_j}^2 \left[\int_{\gamma_{g_j}}^\infty d\gamma_u e^{-\gamma_u/\bar{\gamma}_u} \log(\gamma_u) - \bar{\gamma}_u \log(\bar{\gamma}_R) \right] \\ &\doteq O(\bar{\gamma}_{g_j}^{-1} \bar{\gamma}_R^{-1}),\end{aligned}\quad (52)$$

and

$$\begin{aligned}\Psi_i^2(s, \theta) &= \frac{1}{\bar{\gamma}_{g_j} \bar{\gamma}_R \bar{\gamma}_u} \int_0^\infty d\gamma_R \int_0^{\gamma_R} d\gamma_u \int_0^{\gamma_u} d\gamma_{g_j} e^{-\gamma_{g_j}(\bar{d}_R(\hat{x}_R)s + \frac{\alpha}{\sin^2 \theta} + \frac{1}{\bar{\gamma}_{g_j}})} e^{-\gamma_R/\bar{\gamma}_R} e^{-\gamma_u/\bar{\gamma}_u} \\ &\doteq \frac{\bar{\gamma}_R}{\bar{\gamma}_{g_j} (\bar{\gamma}_R + \bar{\gamma}_u) (\bar{d}_R(\hat{x}_R)s + \frac{\alpha}{\sin^2 \theta})},\end{aligned}\quad (53)$$

respectively. As a result, based on (47)–(49) and (51)–(53) we obtain $\Psi_i(s, \theta) \doteq \Psi_i^1(s, \theta) + \Psi_i^2(s, \theta)$

as

$$\Psi_i(s, \theta) \doteq \begin{cases} O(\bar{\gamma}_{g_j}^{-1} \bar{\gamma}_R^{-1}) & i > 1 \\ O(\bar{\gamma}_{g_j}^{-1} \bar{\gamma}_R^{-1} \log(\bar{\gamma}_u)) & i = 1 \\ \frac{1}{\bar{\gamma}_{g_j} (\bar{d}_R(\hat{x}_R)s + \frac{\alpha}{\sin^2 \theta})} & i = 0 \end{cases} \quad (54)$$

Substituting this result into (41) leads to (38) upon using (39). \blacksquare

Lemma 3: The asymptotic behavior of $I(s) \triangleq \mathcal{E}_{\gamma_{\text{eq}}, \gamma_R, \bar{n}_{D,R}} \{e^{-s\lambda_R \Delta_R(x_R, \tilde{x}_R, x_R)}\}$ for $\bar{\gamma}_{g_i} \rightarrow \infty$, $1 \leq i \leq N_s$, $\bar{\gamma}_R \rightarrow \infty$ is given by

$$I(s) \triangleq \frac{1}{\bar{\gamma}_{\text{eq}} d_R^2 s} - \frac{1}{\bar{\gamma}_R d_R^2 s(s-1)}, \quad (55)$$

for $d_R \neq 0$, while $I(s) = 1$ is valid for $d_R = 0$.

Proof. Since from (40) we have $\lambda_R \Delta_R(x_R, \tilde{x}_R, x_R) = \gamma_m d_R^2 + \frac{2\gamma_m}{\sqrt{\gamma_R}} d_R \Re\{\bar{n}_{D,R}^*\}$, we conclude that $I(s) = 1$ is valid for $d_R = 0$. For $d_R \neq 0$ we use Taylor series expansion $e^x = \sum_{i=0}^{\infty} x^i/i!$ to write $I(s|\bar{n}_{D,R}) \triangleq \mathcal{E}_{\gamma_{\text{eq}}, \gamma_R} \{e^{-s\lambda_R \Delta_R(x_R, \tilde{x}_R, x_R)}\}$ as

$$I(s|\bar{n}_{D,R}) = \mathcal{E}_{\bar{n}_{D,R}} \left\{ \sum_{i=0}^{\infty} \frac{2^i \eta_i}{(2i)!} |\bar{n}_{D,R}|^{2i} s^{2i} \Upsilon_i(s, \theta) \right\}, \quad (56)$$

where

$$\Upsilon_i(s, \theta) \triangleq \mathcal{E}_{\gamma_{\text{eq}}, \gamma_R} \left\{ e^{-\gamma_m d_R^2 s} \left(\frac{\gamma_m d_R}{\sqrt{\gamma_R}} \right)^{2i} \right\} = \frac{d_R^{2i}}{\bar{\gamma}_{\text{eq}} \bar{\gamma}_R} \int_0^{\infty} \int_0^{\infty} e^{-\gamma_m d_R^2 s} \gamma_m^{2i} \gamma_R^{-i} e^{-\gamma_{\text{eq}}/\bar{\gamma}_{\text{eq}}} e^{-\gamma_R/\bar{\gamma}_R} d\gamma_{\text{eq}} d\gamma_R. \quad (57)$$

Splitting the inner integration interval in (57) into two intervals $[0, \gamma_{\text{eq}}]$, $[\gamma_{\text{eq}}, \infty)$ yields $\Upsilon_i(s, \theta) = \Upsilon_i^1(s, \theta) + \Upsilon_i^2(s, \theta)$ where

$$\Upsilon_i^1(s, \theta) \triangleq \frac{d_R^{2i}}{\bar{\gamma}_{\text{eq}} \bar{\gamma}_R} \int_0^{\infty} d\gamma_{\text{eq}} e^{-\gamma_{\text{eq}}/\bar{\gamma}_{\text{eq}}} \int_0^{\gamma_{\text{eq}}} d\gamma_R \gamma_R^i e^{-(\gamma_R d_R^2 s + \gamma_R/\bar{\gamma}_R)}, \quad (58)$$

and

$$\Upsilon_i^2(s, \theta) \triangleq \frac{d_R^{2i}}{\bar{\gamma}_{\text{eq}} \bar{\gamma}_R} \int_0^{\infty} d\gamma_{\text{eq}} \gamma_{\text{eq}}^{2i} e^{-\gamma_{\text{eq}}(d_R^2 s + 1/\bar{\gamma}_{\text{eq}})} \int_{\gamma_{\text{eq}}}^{\infty} d\gamma_R \gamma_R^{-i} e^{-(\gamma_R/\bar{\gamma}_R)}. \quad (59)$$

We find the asymptotic behavior of $\Upsilon_i^1(s, \theta)$ and $\Upsilon_i^2(s, \theta)$, respectively, in the following for $\bar{\gamma}_{\text{eq}}, \bar{\gamma}_R \rightarrow \infty$. For $\Upsilon_i^1(s, \theta)$ we write (58) as

$$\Upsilon_i^1(s, \theta) = \frac{i!}{\bar{\gamma}_R d_R^2 s^{i+1}} - \frac{d_R^{2i}}{\bar{\gamma}_{\text{eq}} \bar{\gamma}_R} \sum_{k=0}^i \int_0^{\infty} \frac{i! \gamma_{\text{eq}}^k e^{(d_R^2 s + 1/\bar{\gamma}_{\text{eq}} + 1/\bar{\gamma}_{\text{eq}})\gamma_{\text{eq}}} }{k! (d_R^2 s + 1/\bar{\gamma}_{\text{eq}})^{i-k+1}} d\gamma_{\text{eq}} \triangleq \frac{i!}{\bar{\gamma}_R d_R^2 s^{i+1}}. \quad (60)$$

For $\Upsilon_i^2(s, \theta)$ we first express (59) as

$$\Upsilon_i^2(s, \theta) = \frac{d_R^i}{\bar{\gamma}_{\text{eq}} \bar{\gamma}_R^i} \int_0^{\infty} d\gamma_{\text{eq}} \gamma_{\text{eq}}^{2i} e^{-\gamma_{\text{eq}}(d_R^2 s + 1/\bar{\gamma}_{\text{eq}})} \Gamma(1-i, \gamma_{\text{eq}}/\bar{\gamma}_R). \quad (61)$$

Following steps similar to those used in Lemma 2 to obtain the asymptotic behavior of $\Psi_i^2(s, \theta)$ we arrive at

$$\Upsilon_i^2(s, \theta) \triangleq \begin{cases} O(\bar{\gamma}_{\text{eq}}^{-1} \bar{\gamma}_R^{-1}) & i > 1 \\ \frac{2 \log(\bar{\gamma}_R)}{d_R^6 s^3 \bar{\gamma}_{\text{eq}} \bar{\gamma}_R} & i = 1 \\ \frac{1}{\bar{\gamma}_{\text{eq}} d_R^2 s} & i = 0 \end{cases} \quad (62)$$

With (60) and (62) for $\Upsilon_i(s, \theta) = \Upsilon_i^1(s, \theta) + \Upsilon_i^2(s, \theta)$ we get

$$\Upsilon_i(s, \theta) \triangleq \begin{cases} \frac{i!}{\bar{\gamma}_R d_R^2 s^{i+1}} & i \geq 1 \\ \frac{1}{d_R^2 s} \left(\frac{1}{\bar{\gamma}_{\text{eq}}} + \frac{1}{\bar{\gamma}_R} \right) & i = 0 \end{cases} \quad (63)$$

Substituting (63) in (56) results in

$$I(s|\bar{n}_{D,R}) = \frac{1}{d_R^2 s} \left(\frac{1}{\bar{\gamma}_{\text{eq}}} + \frac{1}{\bar{\gamma}_R} \right) + \frac{1}{d_R^2 s \bar{\gamma}_R} \sum_{i=1}^{\infty} \frac{2^i i! \eta_i}{(2i)!} |\bar{n}_{D,R}|^{2i} s^i = \frac{1}{d_R^2 s \bar{\gamma}_{\text{eq}}} + \frac{e^{|\bar{n}_{D,R}|^2 s}}{d_R^2 s \bar{\gamma}_R}, \quad (64)$$

where we have used $\eta_i = \frac{(2i)!}{2^i (i!)^2}$. Finally, averaging $I(s|\bar{n}_{D,R})$ over the Rayleigh distributed RV $|\bar{n}_{D,R}|$ leads to (55). ■

Lemma 4: The asymptotic behavior of $\Phi_R^c(s) \triangleq \mathcal{E}_{\gamma_{\text{eq}}, \gamma_R, \bar{n}_{D,R}} \{ [1 - \beta Q(\sqrt{2\alpha \gamma_{\text{eq}}})] e^{-s \lambda_R \Delta_R(x_R, \tilde{x}_R, x_R)} \}$ for $\bar{\gamma}_{g_i} \rightarrow \infty$, $1 \leq i \leq N_s$, $\bar{\gamma}_R \rightarrow \infty$ is given by

$$\Phi_R^c(s) \triangleq \frac{1}{\pi} \int_0^{\pi/2} \left(\frac{2}{\bar{\gamma}_{\text{eq}} d_R^2 s} - \frac{2}{\bar{\gamma}_R d_R^2 s(s-1)} - \frac{\beta}{\bar{\gamma}_{\text{eq}} d_R^2 (s + \frac{\alpha}{\sin^2 \theta d_R^2})} \right) d\theta, \quad (65)$$

for $d_R \neq 0$, while $\Phi_R^c(s) \triangleq 1$ is valid for $d_R = 0$.

Proof. We first note that $\Phi_R^c(s) = I(s) - \sum_{j=1}^{N_s} \Phi_{R,j}^e(x_R; s)$, where we have employed $Q(\sqrt{2\alpha \gamma_{\text{eq}}}) \approx \sum_{i=1}^{N_s} Q(\sqrt{2\alpha \gamma_{g_j}})$ which is valid for $\bar{\gamma}_{g_i} \rightarrow \infty$, $1 \leq i \leq N_s$. For $d_R \neq 0$ combining (38) and (55) readily results in (65). For $d_R = 0$ from (38) and (55) we obtain $\Phi_R^c(s) = 1 - \frac{1}{\pi \bar{\gamma}_{\text{eq}}} \int_0^{\pi/2} \frac{\beta \sin^2 \theta}{\alpha} d\theta \triangleq 1$. ■

Proof. [Proposition 1] Based on Lemma 1 $\Phi_{f_i}(s)$ can be written as $\Phi_{f_i}(s) \triangleq \tilde{k}_1 \bar{\gamma}$ for $x_i \neq \tilde{x}_i$ and $\Phi_{f_i}(s) \triangleq 1$ for $x_i = \tilde{x}_i$, where \tilde{k}_1 is a finite (positive) constant. Furthermore, using Lemmas 2 and 4 in (15) yields $\Phi_R(s) \triangleq \tilde{k}_2 \bar{\gamma}$ for $x_R \neq \tilde{x}_R$ where \tilde{k}_2 is a finite (positive) constant, and $\Phi_R(s) \triangleq 1$ for $x_R = \tilde{x}_R$. Therefore, based on (13) we conclude that $G_{d,\text{PEP}}$ is given by the number of non-zero elements in the vector $[x_1 - \tilde{x}_1, \dots, x_{N_s} - \tilde{x}_{N_s}, x_R - \tilde{x}_R]^T$. Since $\mu_{\mathcal{X}} : \mathcal{A} \rightarrow \mathcal{X}$ is a one-to-one mapping function, $G_{d,\text{PEP}}$ is alternatively given by the Hamming distance between the transmit symbol vectors \mathbf{s}_e and $\tilde{\mathbf{s}}_e$ denoted as $d_H(\mathbf{x}, \tilde{\mathbf{x}})$. To see $d_H(\mathbf{x}, \tilde{\mathbf{x}}) \geq 2$, we first note that by definition we have $\mathbf{x} \neq \tilde{\mathbf{x}}$, and therefore $s_i \neq \tilde{s}_i$ is valid for $i \in \mathcal{I}$, where \mathcal{I} is a non-empty index set. For $|\mathcal{I}| \geq 2$, $d_H(\mathbf{x}, \tilde{\mathbf{x}}) \geq 2$ immediately follows. For $|\mathcal{I}| = 1$ it is easy to see that $s_R \neq \tilde{s}_R$, resulting in $d_H(\mathbf{x}, \tilde{\mathbf{x}}) = 2$. ■

Proof. [Proposition 2] For a given transmit signal vector \mathbf{x} , the set $\mathcal{C}_i(\mathbf{x})$ in (26) can be partitioned into N_s disjoint sets $\mathcal{C}_i^l(\mathbf{x})$, $1 \leq l \leq N_s$, i.e., $\mathcal{C}_i(\mathbf{x}) = \bigcup_{l=1}^{N_s} \mathcal{C}_i^l(\mathbf{x})$, where $\mathcal{C}_i^l(\mathbf{x})$ is defined in (31). Therefore, the asymptotic SER can be calculated by using (5) and (26) as

$$P_s^i \triangleq \frac{1}{M^{N_s}} \sum_{\mathbf{x} \in \mathcal{X}^{N_s}} \sum_{l=1}^{N_s} \sum_{\tilde{\mathbf{x}} \in \mathcal{C}_i^l(\mathbf{x})} P(\mathbf{x} \rightarrow \tilde{\mathbf{x}}). \quad (66)$$

For $\tilde{\mathbf{x}} \in \mathcal{C}_i^i(\mathbf{x})$, the asymptotic PEP can be obtained from (20) and (22) as

$$P(\mathbf{x} \rightarrow \tilde{\mathbf{x}}) \doteq \frac{1}{\bar{\gamma}_{f_i}} \left(\phi_c^g(\mathbf{x}, \tilde{\mathbf{x}}) \sum_{j=1}^{N_s} \frac{1}{\bar{\gamma}_{g_j}} + \frac{\phi_c^R(\mathbf{x}, \tilde{\mathbf{x}})}{\bar{\gamma}_R} \right) + \sum_{j=1}^{N_s} \frac{1}{|\mathcal{D}_j(\mathbf{x})|} \sum_{\hat{\mathbf{x}}_R \in \mathcal{D}_j(\mathbf{x})} \frac{\phi_e(\mathbf{x}, \tilde{\mathbf{x}}, \hat{\mathbf{x}}_R)}{\bar{\gamma}_{f_i} \bar{\gamma}_{g_j}}. \quad (67)$$

For $\tilde{\mathbf{x}} \in \mathcal{C}_i^l(\mathbf{x})$, $l \neq i$, using (24) and (25) yields

$$P(\mathbf{x} \rightarrow \tilde{\mathbf{x}}) \doteq \frac{\bar{\phi}_c(\mathbf{x}, \tilde{\mathbf{x}})}{\bar{\gamma}_{f_i} \bar{\gamma}_{f_l}} + \sum_{j=1}^{N_s} \frac{1}{|\mathcal{D}_j(\mathbf{x})|} \sum_{\hat{\mathbf{x}}_R \in \mathcal{D}_j(\mathbf{x})} \frac{\bar{\phi}_e(\mathbf{x}, \tilde{\mathbf{x}}, \hat{\mathbf{x}}_R)}{\bar{\gamma}_{f_i} \bar{\gamma}_{f_l} \bar{\gamma}_{g_j}} \doteq \frac{\bar{\phi}_c(\mathbf{x}, \tilde{\mathbf{x}})}{\bar{\gamma}_{f_i} \bar{\gamma}_{f_l}}. \quad (68)$$

(27) can now be obtained by combining (66), (67), and (68). ■

References

- [1] J.N. Laneman, D.N.C. Tse, and G.W. Wornell. "Cooperative Diversity in Wireless Networks: Efficient Protocols and Outage Behavior". *IEEE Trans. Inform. Theory*, 50:3062–3080, December 2004.
- [2] Y. Chen, S. Kishore, and J. Li. "Wireless Diversity Through Network Coding". In *Proc. IEEE Wireless Commun. and Networking Conf. (WCNC)*, volume 3, pages 1681–1686, 2006.
- [3] M. Yu, J. Li, and R.S. Blum. "User Cooperation Through Network Coding". In *Proc. IEEE Inter. Conf. Commun. (ICC)*, pages 4064–4069, 2007.
- [4] C. Peng, Q. Zhang, M. Zhao, Y. Yao, and W. Jia. "On the Performance Analysis of Network-Coded Cooperation in Wireless Networks". *IEEE Trans. Wireless Commun.*, 7:3090–3097, August 2008.
- [5] R. Ahlswede, N. Cai, S. Li, and R. Yeung. "Network Information Flow". *IEEE Trans. Inform. Theory*, 46:1204–1216, July 2000.
- [6] L. Xiao, T.E. Fuja, J. Kliewer, and D.J. Costello. "A Network Coding Approach to Cooperative Diversity". *IEEE Trans. Inform. Theory*, 53:3714–3722, October 2007.
- [7] A. Cano, T. Wang, A. Ribeiro, and G.B. Giannakis. "Link-Adaptive Distributed Coding for Multi-Source Cooperation". *EURASIP J. on Adv. in Signal Process.*, 2008:1–12, January 2008.
- [8] S. Zhang, S.C. Liew, and P.P. Lam. "Hot topic: Physical-Layer Network coding". In *Proceedings of 12th Annual International Conference on Mobile Computing and Networking (MobiCom)*, pages 358–365, September 2006.
- [9] T. Wang and G.B. Giannakis. "Complex Field Network Coding for Multiuser Cooperative Communications". *IEEE J. Select. Areas Commun.*, 26:561–571, April 2008.
- [10] T. Wang, A. Cano, G.B. Giannakis, and J.N. Laneman. "High-Performance Cooperative Demodulation With Decode-and-Forward Relays". *IEEE Trans. Commun.*, 55:1427–1438, July 2007.
- [11] S. Lin and J.J. Costello. *Error Control Coding*. Prentice Hall, Englewood Cliffs, New Jersey, 1983.
- [12] S. Lin, T. Kasami, T. Fujiwara, and M. Fossorier. *Trellises and Trellis-Based Decoding Algorithms for Linear Block Codes*. Kluwer, Norwell, MA, 1998.
- [13] A. Nasri, R. Schober, and I.F. Blake. "Performance and Optimization of Cooperative Diversity Systems in Generic Noise and Interference". *Submitted to the IEEE Trans. Wireless Commun.*, available at: <http://www.ece.ubc.ca/~amirn/TW09.pdf>, 2010.
- [14] K.T. Phan, T. Le-Ngoc, S.A. Vorobyov, and C. Tellambura. "Power Allocation in Wireless Relay Networks: A Geometric Programming-Based Approach". In *Proceedings of the IEEE Global Telecommun. Conf. (Globecom)*, pages 1–5, 2008.
- [15] S. Boyd and L. Vandenberghe. *Convex Optimization*. U.K.: Cambridge Univ. Press, 2004.
- [16] A. Nasri and R. Schober. "Performance of BICM-SC and BICM-OFDM Systems with Diversity Reception in Non-Gaussian Noise and Interference". *IEEE Trans. Commun.*, pages 3316–3327, November 2009.

Figures:

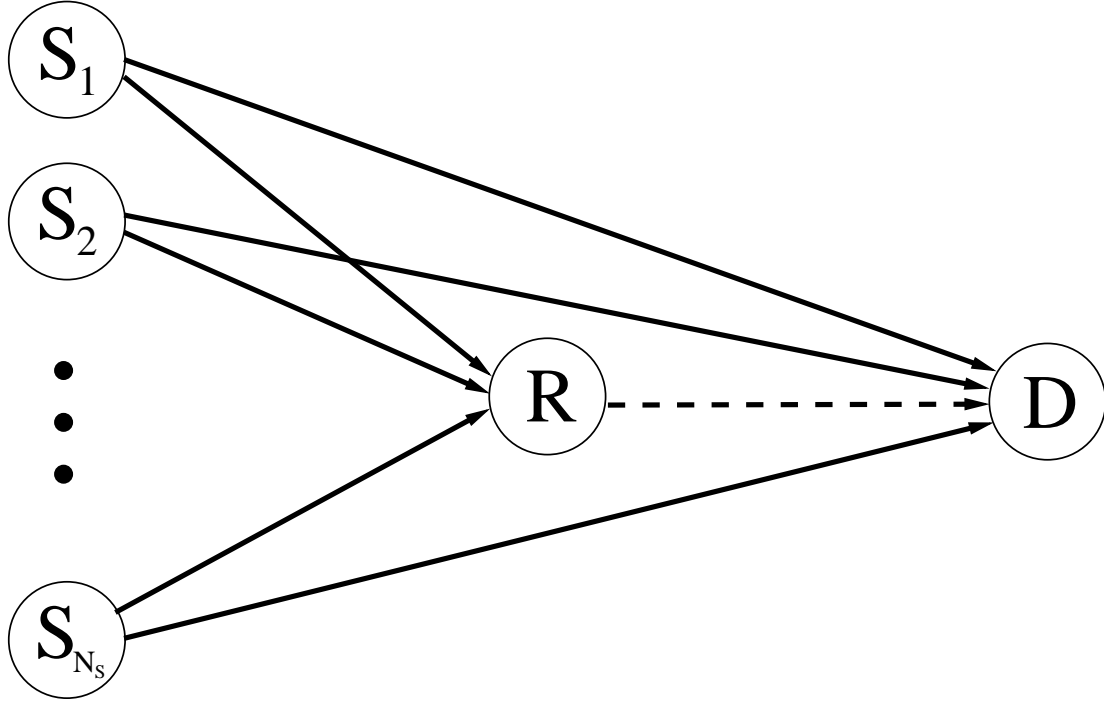


Figure 1: Block diagram of the considered NCCD system. Solid and dashed lines denote links belonging to first and second hop, respectively.

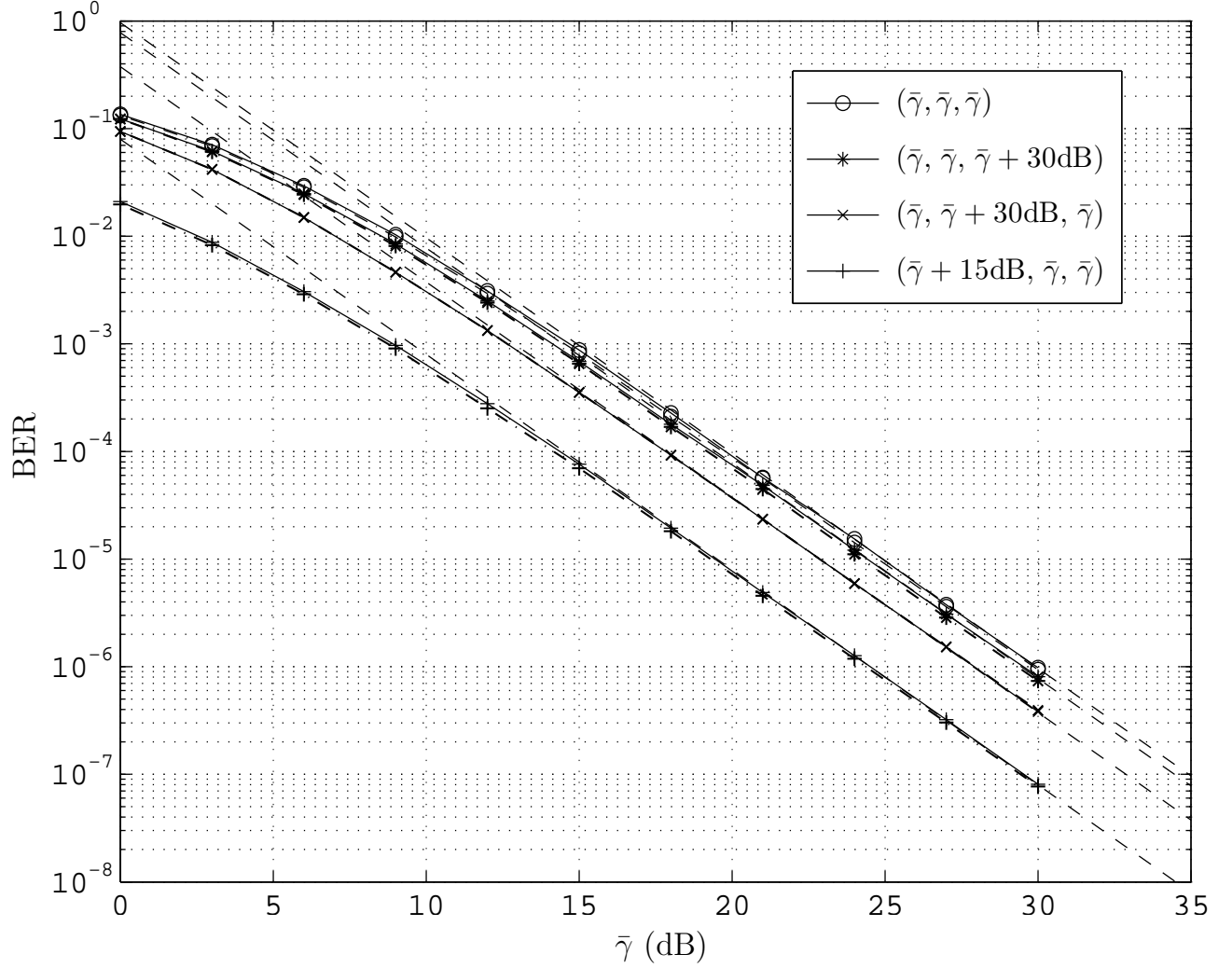


Figure 2: BER of a symmetric NCCD system with $N_s = 2$ sources and BPSK modulation vs. $\bar{\gamma}$ for various channel qualities settings $(\bar{\gamma}_f, \bar{\gamma}_g, \bar{\gamma}_R)$. Solid lines with markers: Simulated BER. Dashed line: Asymptotic BER. Dash-dotted lines with markers: Simulated BER for ML diversity combining at the destination.

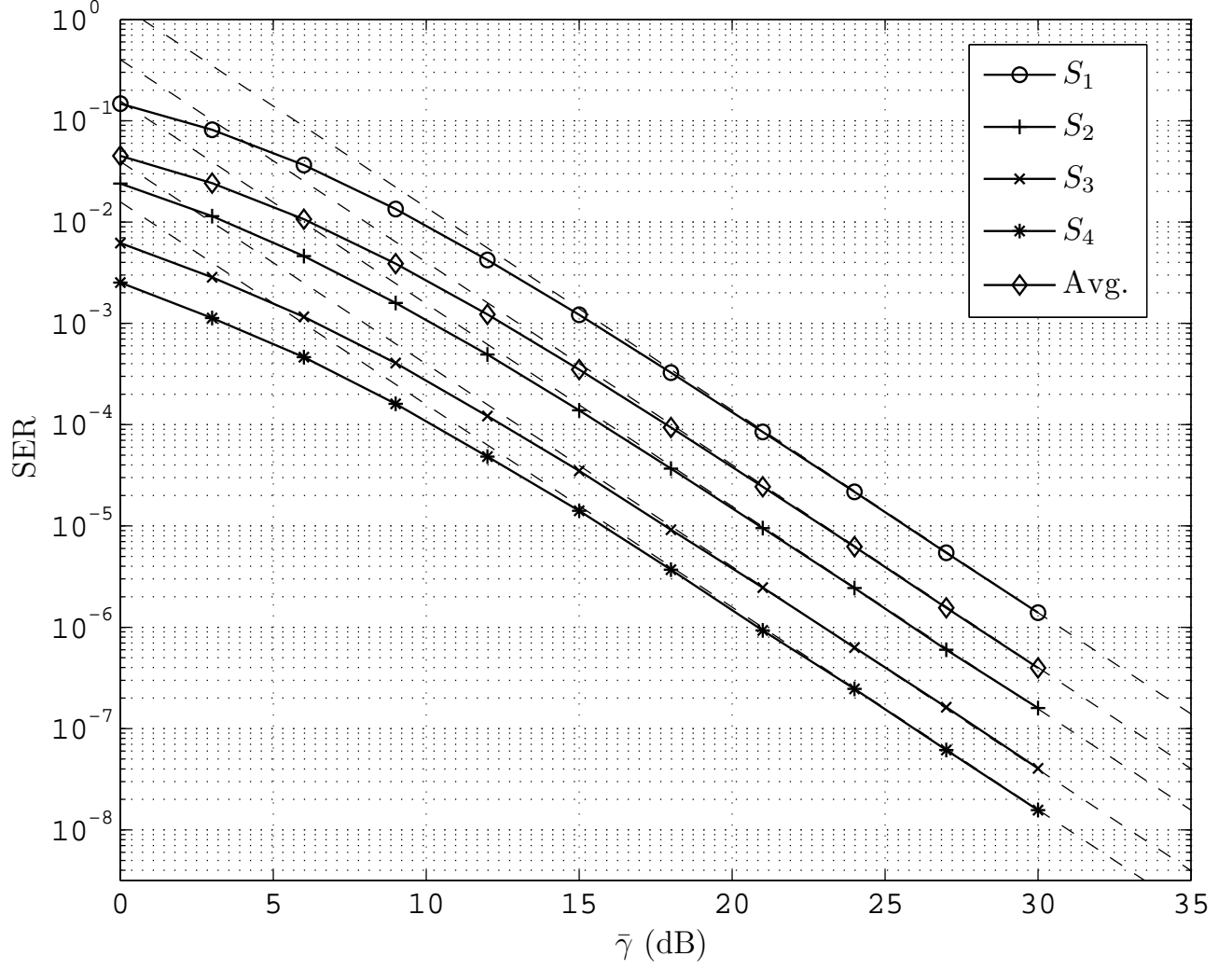


Figure 3: BER vs. $\bar{\gamma}$ for an asymmetric NCCD system with $N_s = 4$ sources and BPSK modulation. Solid lines with markers: Simulated BER. Dashed line: Asymptotic BER.

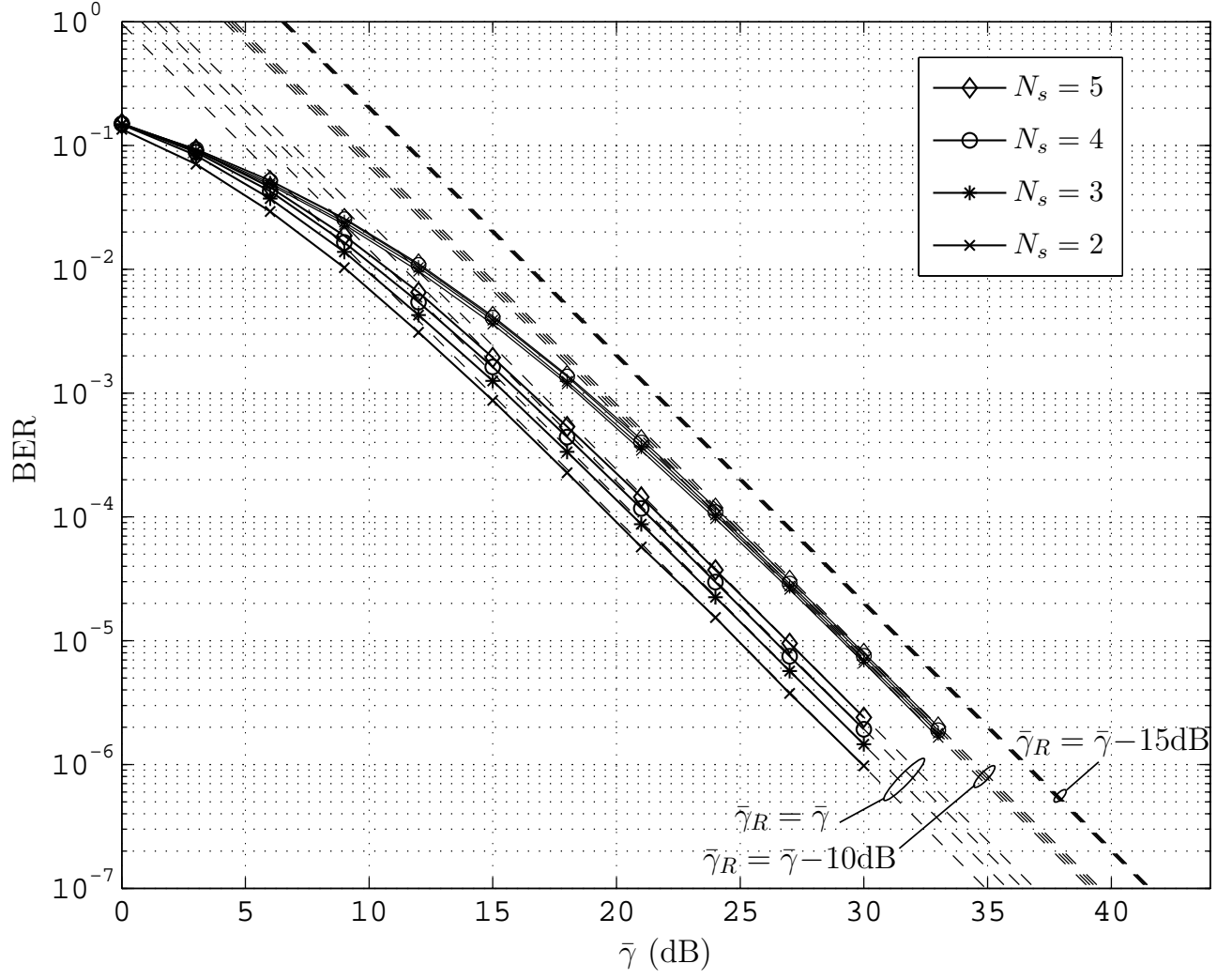


Figure 4: BER of a NCCD system with BPSK modulation vs. $\bar{\gamma}$ for different N_s . Solid lines with markers: Simulated BER. Dashed line: Asymptotic BER.

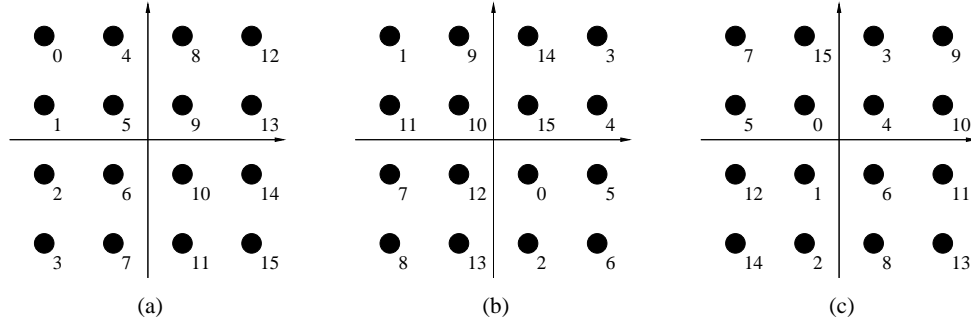


Figure 5: 16-QAM signal constellation with three different constellation mappings $\mu_{\mathcal{X}} : \mathcal{A} \rightarrow \mathcal{X}$. (a) A natural mapping, (b) Optimal mapping for Case I, and (c) Optimal mapping for Case II.

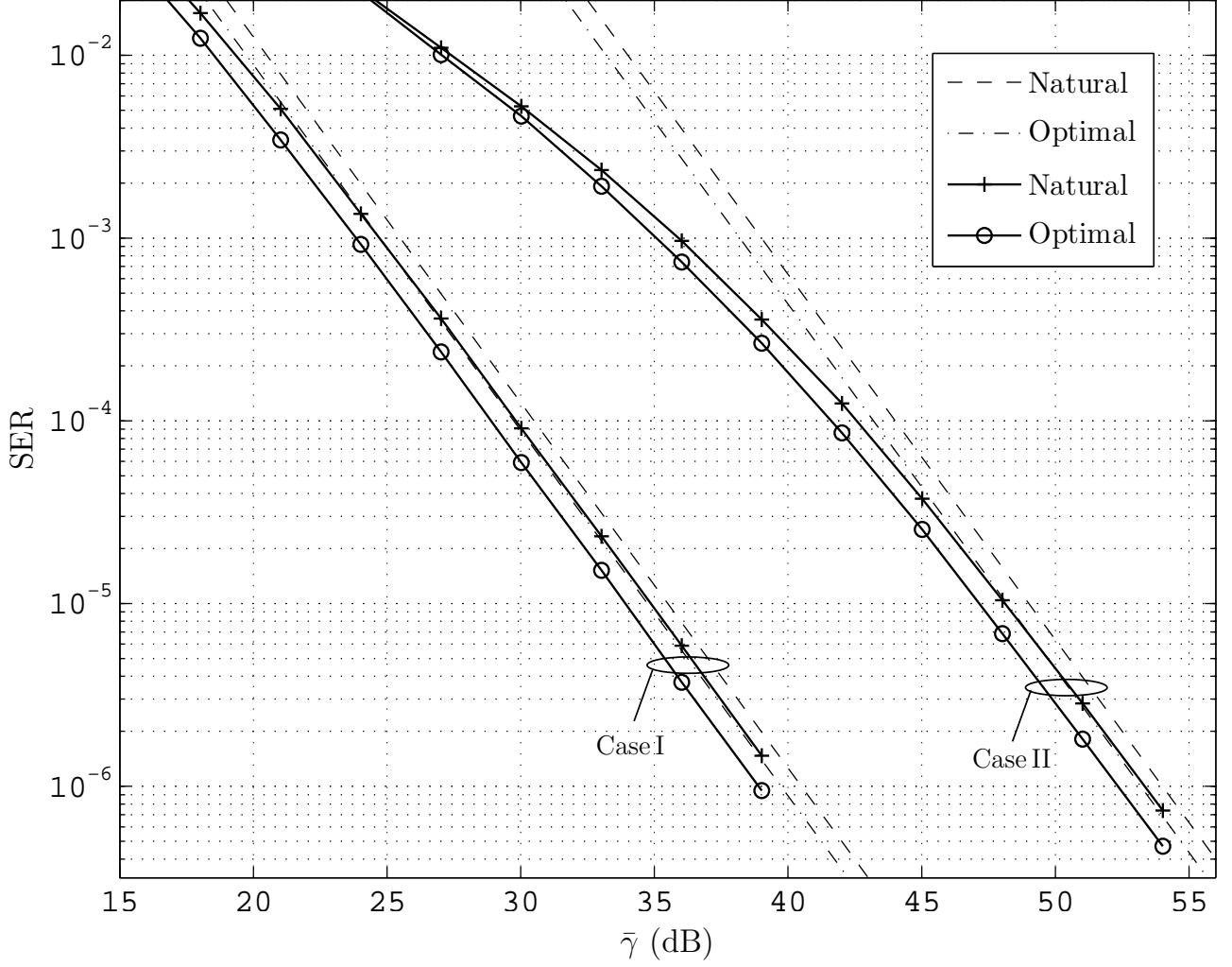


Figure 6: SER of a NCCD system with 16-QAM modulation and $N_s = 2$ for the optimal and natural mappings depicted in Fig. 5 in two channel quality settings Case I and Case II. Solid lines with markers: Simulated SER. Dashed line: Asymptotic SER for natural mapping. Dash-dotted line: Asymptotic SER for optimal mapping.

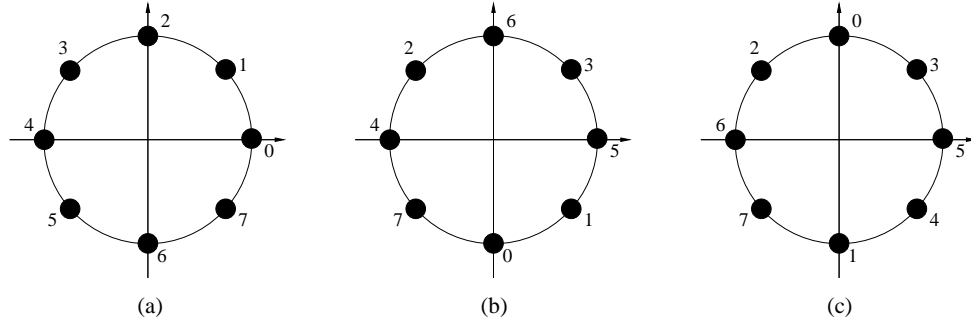


Figure 7: 8-PSK signal constellation with three different constellation mappings $\mu_{\mathcal{X}} : \mathcal{A} \rightarrow \mathcal{X}$. (a) A natural mapping, (b) Optimal mapping for Case I, and (c) Optimal mapping for Case II.

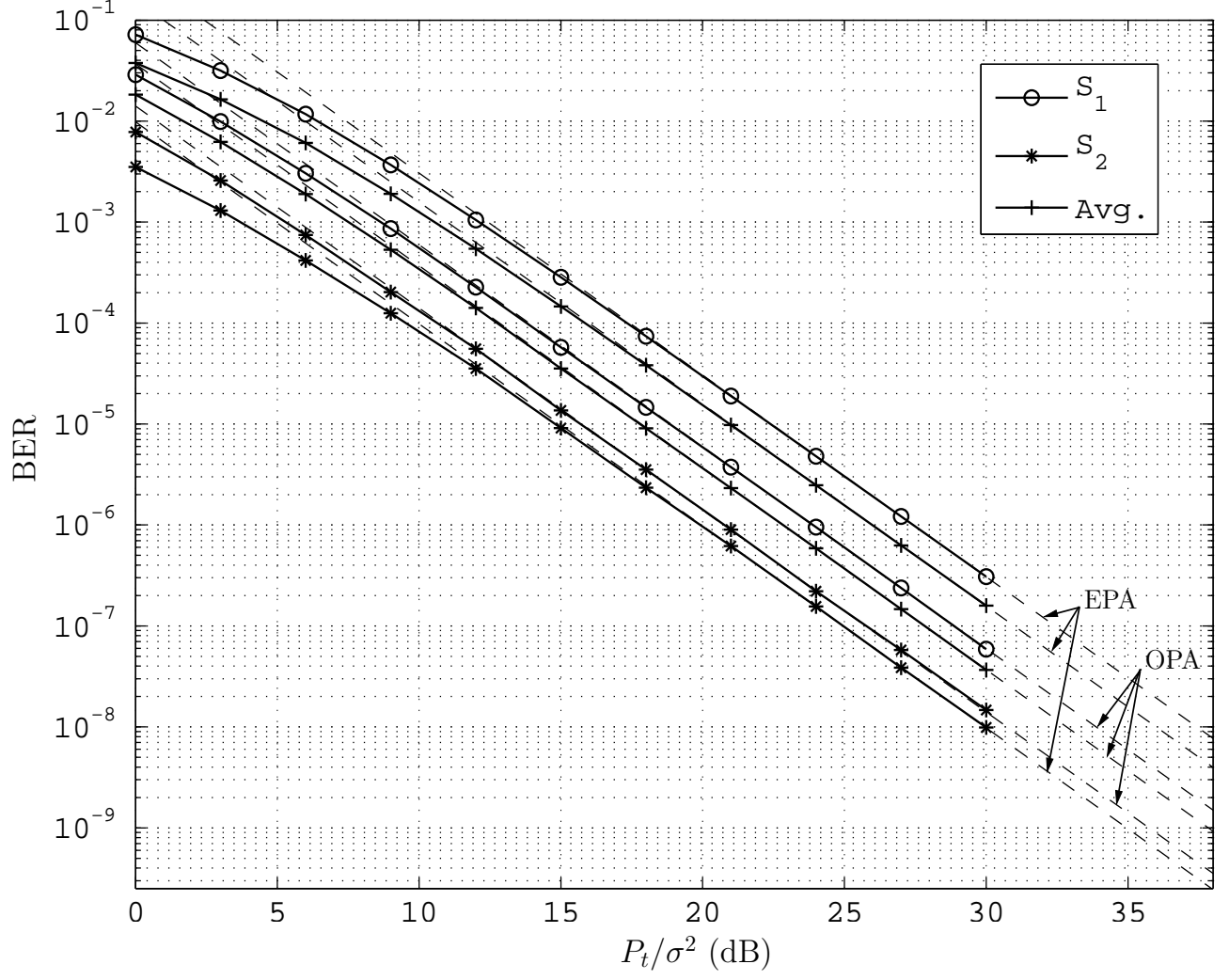


Figure 8: BER vs. P_t/σ^2 of a NCCD system with $N_s = 2$ and BPSK modulation for max-min fair OPA and EPA. Solid lines with markers: Simulated BER. Dashed line: Asymptotic BER.